



LUND UNIVERSITY

Stress and Deformation Characteristics of Concrete at High Temperatures. 2. Experimental Investigation and Material Behaviour Model

Anderberg, Yngve; Thelandersson, Sven

1976

[Link to publication](#)

Citation for published version (APA):

Anderberg, Y., & Thelandersson, S. (1976). *Stress and Deformation Characteristics of Concrete at High Temperatures. 2. Experimental Investigation and Material Behaviour Model*. (Bulletin of Division of Structural Mechanics and Concrete Construction, Bulletin 54; Vol. Bulletin 54). Lund Institute of Technology.

Total number of authors:

2

General rights

Unless other specific re-use rights are stated the following general rights apply:

Copyright and moral rights for the publications made accessible in the public portal are retained by the authors and/or other copyright owners and it is a condition of accessing publications that users recognise and abide by the legal requirements associated with these rights.

- Users may download and print one copy of any publication from the public portal for the purpose of private study or research.
- You may not further distribute the material or use it for any profit-making activity or commercial gain
- You may freely distribute the URL identifying the publication in the public portal

Read more about Creative commons licenses: <https://creativecommons.org/licenses/>

Take down policy

If you believe that this document breaches copyright please contact us providing details, and we will remove access to the work immediately and investigate your claim.

LUND UNIVERSITY

PO Box 117
221 00 Lund
+46 46-222 00 00

YNGVE ANDERBERG – SVEN THELANDERSSON

STRESS AND DEFORMATION CHARACTERISTICS OF CONCRETE AT HIGH TEMPERATURES

2. EXPERIMENTAL INVESTIGATION AND MATERIAL BEHAVIOUR MODEL

LUND INSTITUTE OF TECHNOLOGY LUND SWEDEN 1976

DIVISION OF STRUCTURAL MECHANICS AND CONCRETE CONSTRUCTION

STRESS AND DEFORMATION CHARACTERISTICS OF CONCRETE AT HIGH
TEMPERATURES

2. EXPERIMENTAL INVESTIGATION AND MATERIAL BEHAVIOUR MODEL

Yngve Anderberg

Sven Thelandersson

LUND, AUGUST 1976

Contents

Preface	3
1 INTRODUCTION	5
2 EXPERIMENTS	8
2.1 Testing equipment	8
2.1.1 Heating	8
2.1.2 Load application	9
2.1.3 Deformation measurements	12
2.1.4 Weight loss measurements	14
2.2 Specimens and materials	16
2.3 Test program	18
2.3.1 Test series A	20
2.3.2 Test series B	22
2.3.3 Test series C	22
2.3.4 Test series D	22
3 TEST RESULTS	27
3.1 Temperatures	27
3.2 Weight loss	27
3.3 Heating to failure under constant stress (test series A)	34
3.4 Stress-strain relations at high temperatures	38
3.5 Creep at constant temperature	44
4 CONSTITUTIVE MODEL	51
4.1 Thermal strain	52
4.2 Instantaneous, stress-related strain	53
4.2.1 Ultimate stress σ_u	55
4.2.2 Ultimate strain ϵ_u	56
4.2.3 Slopes of descending branch	58
4.2.4 Variable stress and temperature	59
4.3 Creep strain ϵ_{cr}	60
4.4 Transient strain ϵ_{tr}	61
4.5 Material behaviour under cooling	64
4.6 Validity of the model	67
5 EXAMPLE CALCULATIONS	74
6 CONCLUSIONS	81
REFERENCES	83

Preface

This paper is the second and final report from a research project carried out at Lund Institute of Technology, Division of Structural Mechanics and Concrete Construction and sponsored by the Swedish Council of Building Research. The authors wish to thank the Council for this support.

A part of the experimental investigation was made as a graduate work by Åke Karlsson and Gunnar Sahlin.

The objective of the research is to provide the experimental and theoretical basis for the analysis of stresses and deformations of concrete subjected to high temperatures. The first part of the project embraced a general discussion of the problems and a critical review of literature and gave a background for the planning of the experimental investigation. This second and final part contains the experimental investigation and a material behaviour model of concrete at transient high temperature conditions, developed on a phenomenological level.

The work on this project is carried out in close cooperation between the authors. This particular report has been outlined and written by the authors in close connection, though Yngve Anderberg has been mainly responsible for the performance of the tests and the theoretical analysis.

The authors want to thank Professor Ove Pettersson, head of the division for his encouraging support and for engaging discussions about this matter. Thanks are also due to C.J. Roslund at the Central Laboratory of Högabä AB, to the whole staff of the division for exchange of thoughts and practical help, and in particular the persons listed below.

Bertil Nilsson and Leif Ljungquist manufactured the testing rig

Karl Erik Bohlin made most of the specimens

Thord Lundgren assisted in measurement problems

Kjell Andersson, Sven-Ingvar Granemark and Tibor Walter assisted in the performance of the tests

Bo Zadig made the drawings

Lisbeth Henning, Tarja Aunola and Karin Lagergren-Petersson typed the manuscript.

The lack of a thorough understanding of the structural behaviour of reinforced and prestressed concrete structures under thermal exposure has become increasingly obvious in recent years. In the structural fire protection field a performance based design procedure has been developed for steel structures /1/, whereas for concrete structures the design is made in a very schematic way /2/. The thermal properties of concrete and the dimensions of concrete structures lead to the development of high temperature gradients, which may give rise to considerable thermal stresses. These stresses may or may not influence the ultimate load-bearing capacity, and it is necessary in many cases to carry out a stress analysis in more or less detail. Any attempt to make such an analysis requires knowledge of the mechanical properties of the materials, a knowledge which is insufficient at present as far as concrete is concerned.

In an earlier paper by the authors /3/ the state of the art was reported as regards the mechanical behaviour of concrete at high temperatures. It was concluded that the present knowledge does not enable us to make a realistic analysis of stresses and deformations in heated, loaded concrete. The fact that data from tests performed at constant temperature cannot solely be used in predicting deformations under transient conditions, means that conventional rheological models can not adequately describe the behaviour.

The deformation behaviour was studied for concrete under torsional loading in /4/ and a theoretical model, capable of predicting the deformations under various temperature and loading conditions, was established. The model was formulated in terms of three strain components, viz. elastic strain, constant temperature creep and transient strain. The elastic strain is explicitly seen as the instantaneous response on a load applied at constant temperature and the constant temperature creep is the time-dependent strain being measured under constant load and constant temperature. The transient strain component is the response on a temperature increase in concrete under stress and thus takes into account the effect of temperature change on the deformation demonstrated in /4, 5, 6 and 11/.

In /4/ the latter component was regarded as time-independent, although the response may in fact be somewhat delayed. It should be noted that the transient component as it was defined in /4/ only occurs if the concrete is stressed while the temperature increases, and should not be confused with the thermal dilatation which is independent of the applied stress. When extending the model to uniaxial compression or tension the thermal expansion - including shrinkage - must be added to the three said components. A realistic model of concrete in compression is also more complicated due to the influence of stress history on the behaviour, which must be taken into account.

The purpose with the present paper is to establish a theoretical model for the mechanical behaviour of concrete in compression under transient temperature conditions. The tests reported herein have been designed to give a qualitative as well as quantitative basis for the formulation of such a model. A reasonably complete picture of the behaviour can be obtained if the following three combinations of stress (σ) and temperature (T) histories are tested:

- A. $\dot{\sigma} = 0$, $\dot{\theta} > 0$ (heating to failure at constant stress)
- B. $\dot{\sigma} > 0$, $\dot{\theta} = 0$ (loading to failure at constant temperature)
- C. $\dot{\sigma} = 0$, $\dot{\theta} = 0$ (creep at constant temperature)

From the second we obtain the stress-strain relations at different temperatures and from the third the constant temperature creep, whereas the first gives us the strains developing under increasing temperature.

The scope of the investigation is concentrated upon temperature conditions that are typical for fire exposure, i.e. relatively rapid heating in the temperature range up to 800°C. This means that the evaporable water disappears rather soon in most of the tests and its influence on the deformations is relatively limited. In the temperature range below 200°C the influence of moisture is probably more marked, and the complex interaction between temperature and moisture flow (which depends on the geometry of the specimen) may have to be considered. This is however beyond the scope of this

paper and the problem is therefore only examined to a limited degree by varying the initial moisture content.

This paper consists of two main parts, firstly, a description of the experimental investigation and test results, and secondly, a formulation and description of a constitutive model valid for heated, stressed concrete. The model is entirely based on the behaviour found in the three types of tests (A - C) mentioned above. An independent check of its validity is made against a series of other tests, with different conceivable stress and temperature histories. The model is finally applied on a centrically loaded circular column subjected to symmetrical thermal exposure, to illustrate its significance in a simple case.

2 EXPERIMENTS

2.1 Testing Equipment

The measurement of deformations at high temperatures involves in several aspects difficult technical problems and the final form and function of the equipment, described in what follows, is the result of a series of improvements and modifications made during the development of the test technique. The test set up, shown in fig 1, comprises a cylindrical furnace, a hydraulic testing machine (maximum loading capacity 1 MN) with a support arrangement for load application and a specially designed device for deformation measurements.

2.1.1 Heating

A cylindrical furnace, constructed at the Central Laboratory at Höganäs AB, was used for the experiments. The furnace, shown in fig 1, was made of refractory bricks of the type "Porosil" and covered with sheet steel to protect it against external wear. The height of the furnace is 0.65 m and the external and internal diameters are 0.50 and 0.12 m respectively. The electrical heating unit consists of spirals made of a high temperature alloy of the type Kanthal Super, embedded in and protected by refractory mortar. The spirals are symmetrically located at the inner surface on a vertical length of 0.30 m, and they are applied and installed in such a way that the furnace can be separated into two identical parts.

The furnace temperature is regulated by an automatic programming device, capable of following an arbitrary chosen time-temperature curve. The programming unit consists of a curve follower (Leeds & Northrup, type Trendtrak), a temperature recorder (L & N, type Speedomax H) and a proportional band control unit (L & N, D.A.T. Series 60). The curve follower consists of a photoelectric detector following the desired time-temperature curve drawn in black ink on a chart. The proportional band action means in effect that the durations of "on" and "off" times in the furnace vary within a specified interval around the set temperature in proportion to the difference between the set temperature and the actual working temperature. In this way oscillations

are avoided and within the limits set by the furnace characteristics a desired time-temperature curve is followed with an accuracy of approximately $\pm 20^{\circ}\text{C}$. The thermocouple connected to the programming unit was placed midheight on the side of the specimen, in contact with the surface but unprotected.

The maximum operating temperature of the furnace is 1200°C , but in the experiments the upper limit is only 800°C . The maximum rate of heating is varying with the working temperature level from $25^{\circ}\text{C} \cdot \text{min}^{-1}$ during the first 7 minutes to $5^{\circ}\text{C} \cdot \text{min}^{-1}$ above $500 - 600^{\circ}\text{C}$.

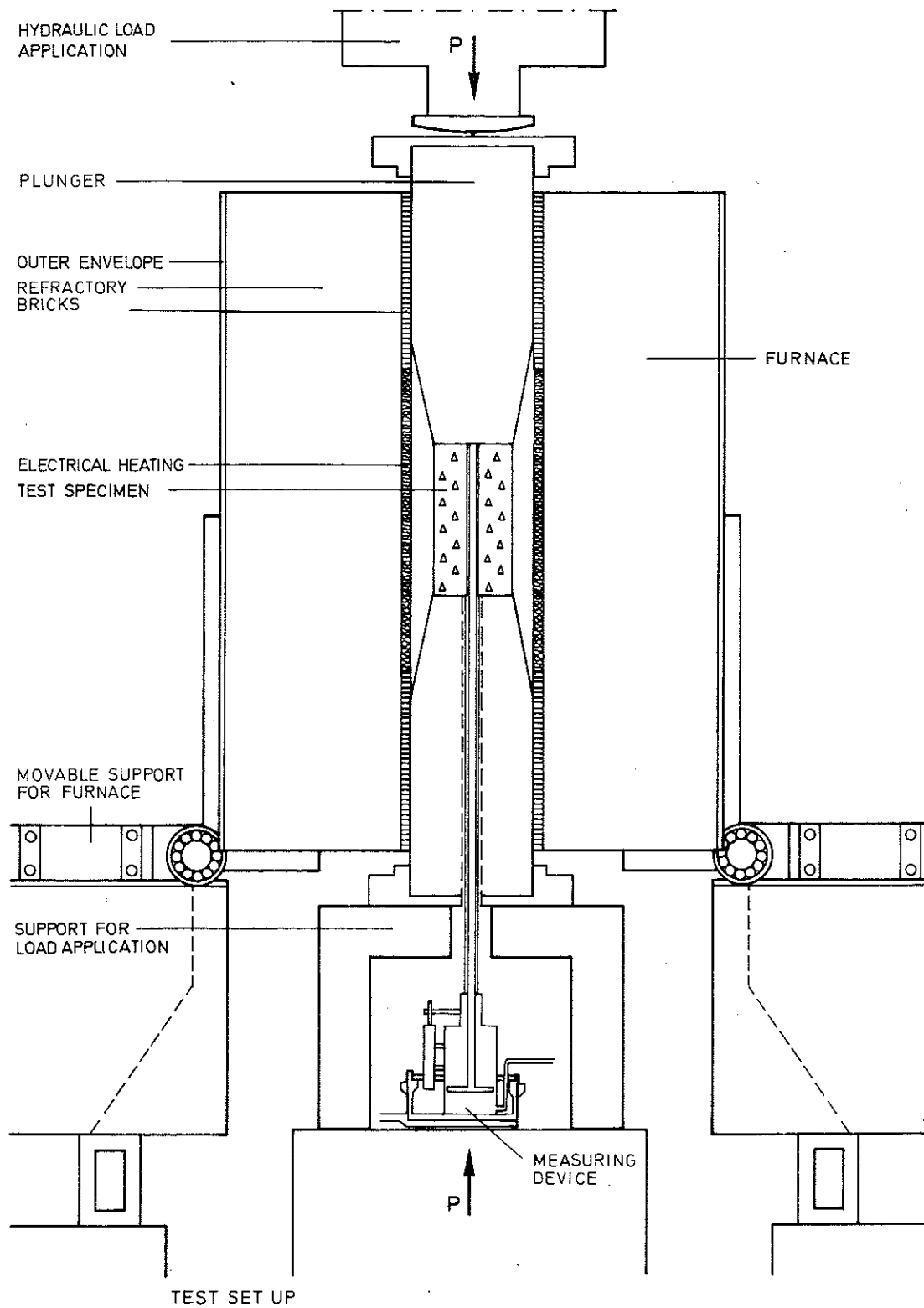
The temperatures in the test specimens were measured in three points by Chromel-Alumel thermocouples (20 AWG, 0.81 mm in diameter, (response time see /14/)) and recorded continuously on two-channelled Servogor printers. Two of the thermocouples were situated at the surface of the inner hole in the specimen, the one at the mid section and the other at the top, whereas the third one was placed about 10 mm from the heated surface in the mid section. The furnace temperature and occasionally the temperature in the inner hole adjacent to the quartz tube were also measured.

The time required for the specimen to attain a uniform temperature distribution after the furnace temperature has reached the desired level, was determined in preliminary tests. A time period of 2 hrs was sufficient to give a reasonably uniform temperature distribution, although a certain temperature deviation within the specimen could not be avoided.

A certain nonuniformity in the longitudinal direction was also observed, but the temperature difference between the top and the mid section was as a rule less than 20°C .

2.1.2 Load application

The whole testing arrangement was placed in a hydraulic testing machine, see fig 1. Centrical loading is accomplished by a spherical bearing in the upper pressure head of the testing machine. The compressive load is transferred to the specimens via plungers made of refractory material (Aluminium oxide, Höganäs AB, type Viktor Korund). This material exhibits high strength at high temperatures (softening temperature = 1700°C) and comparatively low thermal conductivity.



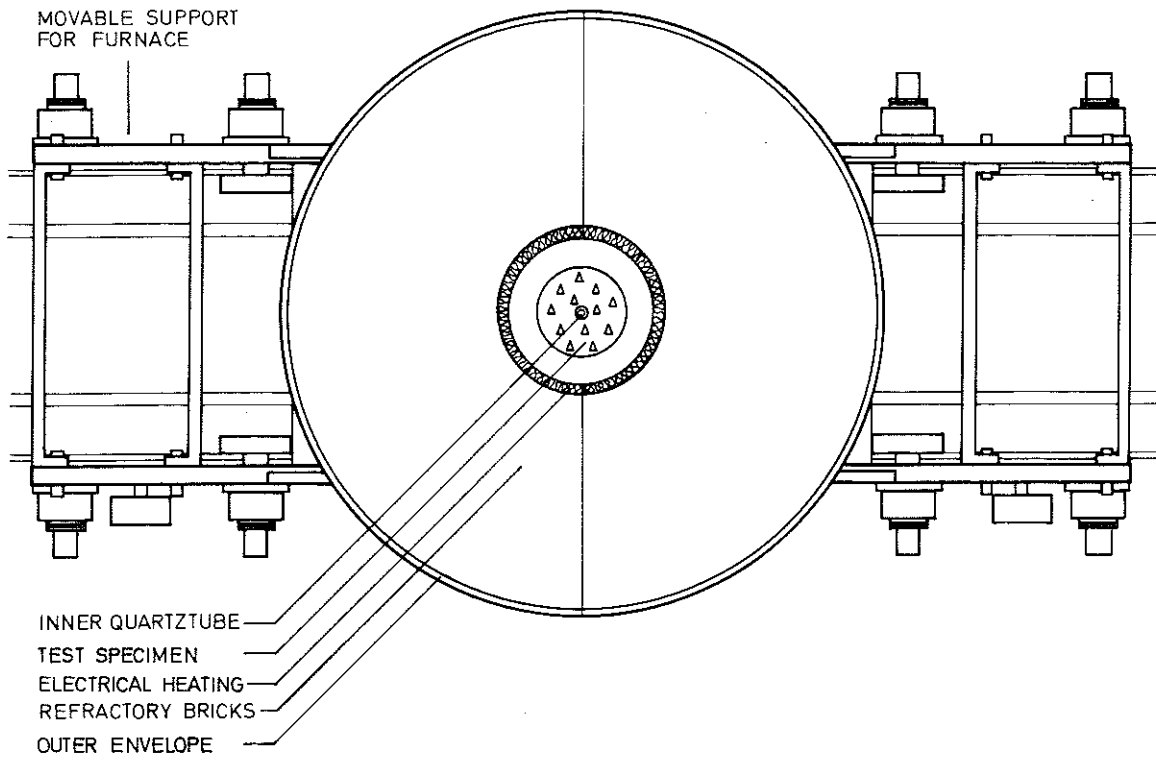


Fig 1 Test equipment.

A pressure transducer (AB Bofors, TDS-2) was installed in the hydraulic system of the testing machine and connected to a printer giving a continuous reading of the applied load.

2.1.3 Deformation measurements

The displacements of the specimen were transferred mechanically out from the furnace with the aid of two quartz tubes with the diameters 8 and 12 mm respectively. Both tubes pass through a 15 mm central hole in the lower plunger. The smaller tube runs inside the larger one, through the 10 mm center hole in the specimen and rests on the top of the specimen, while the larger tube rests on the bottom surface of the specimen, as seen in fig 1.

Both tubes are connected with the measuring device (shown in fig 2), placed underneath the support of load application, where two pistons give the respective tubes a constant upward pressure.

This method of measuring the deformation along the entire length of the specimen creates some problems in the initial stages of loading. The end effects originating from lacking planeness of the surfaces may give rise to errors in the measured strain upon initial loading. In order to avoid this the specimen was loaded to a certain small level and then unloaded prior to testing.

In fig 2 is also shown the arrangement for drainage of the water dripping down along the quartz tubes. The water flow is a result of the transport of evaporable water in the concrete specimen towards the centre during heating.

The movement of the quartz tubes relative to each other was measured by a linear motion potentiometer, type CIC, with very high resolution. The deviation from linearity is estimated to maximum ± 0.015 mm if a measuring length of 1 mm (≈ 7 $^{\circ}$ /oo) is used. If the totally measured length is smaller the error is also smaller, though not proportionally.

A regulated power control and a device for zero adjustment was designed for the potentiometer. The power control provides a very

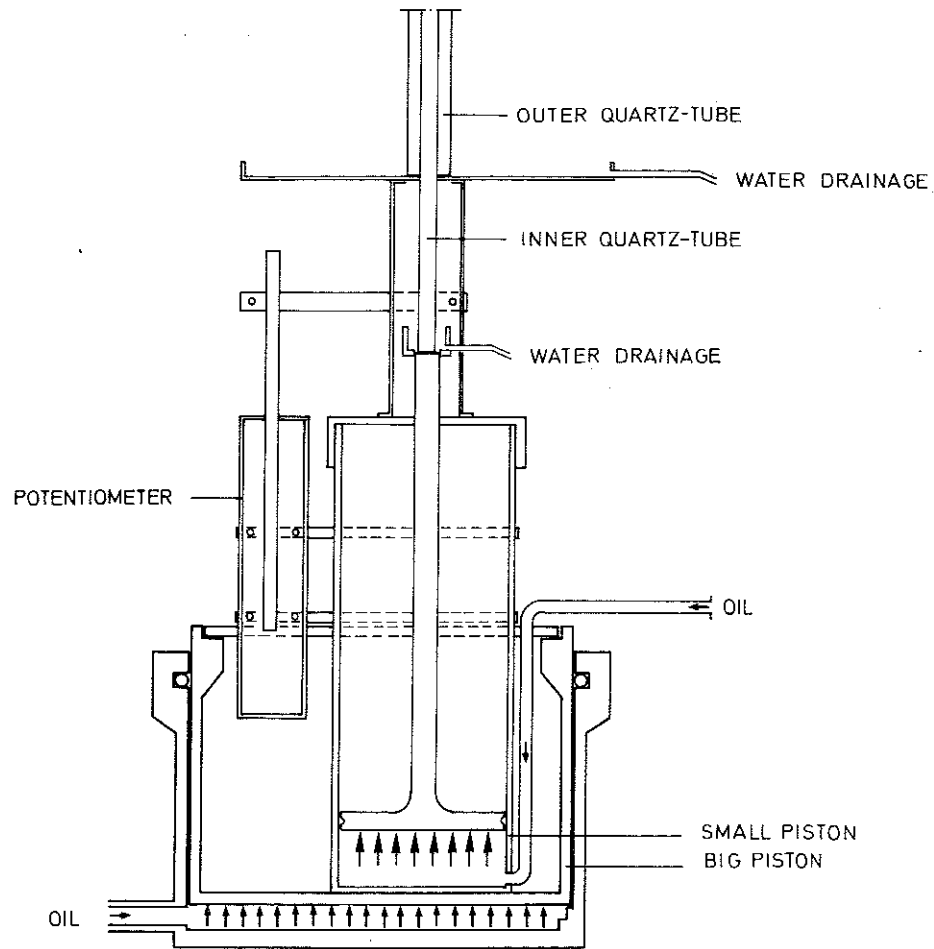


Fig 2 Equipment for deformation measurements.

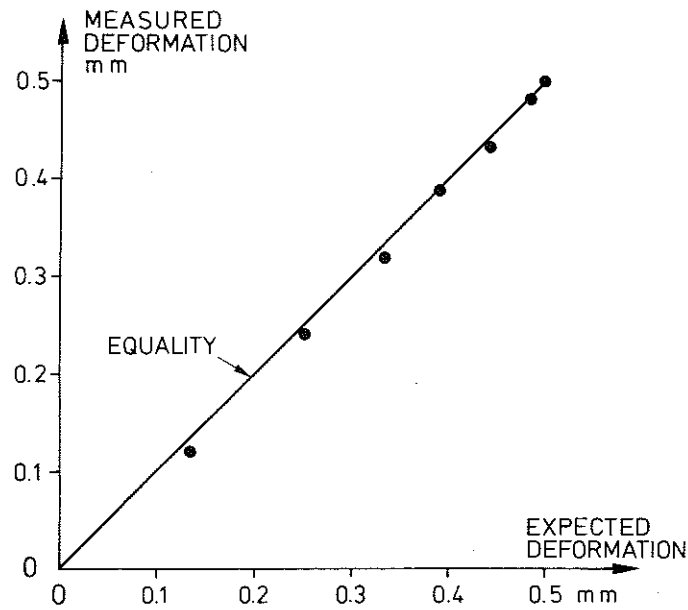


Fig 3 Comparison between measured and expected elongation of steel tube.

high accuracy and the precision of the potentiometer is therefore preserved. The measured deformation were recorded continuously on a Servogor printer, giving the voltage with a guaranteed accuracy of $\pm 0.5\%$ in the actual measuring range. Totally, the relative error for a measured strain of $5 \text{ }^{\circ}/\text{oo}$ or more is estimated to be less than $\pm 2\%$ of the measured strain.

Under non-steady temperature conditions the measured strains had to be corrected for the thermal elongation of the quartz tubes. This correction is rather small since the coefficient of thermal expansion of the quartz only amounts to $0.6 \cdot 10^{-6} \text{ }^{\circ}\text{C}^{-1}$, which is less than about 5% of that of concrete.

The reliability of the measured deformations was checked in preliminary tests on a steel tube with the same external diameter as the concrete specimens. The steel tube was heated to different temperature levels and the measured elongation was compared with the elongation of the steel given from other sources. In fig 3 is shown such a comparison when the steel tube was heated at $5^{\circ}\text{C} \cdot \text{min}^{-1}$ to 275°C where the temperature was stabilized. The expected deformation is taken from /7/. The differences are practically negligible even during the heating phase.

2.1.4 Weight loss measurements

The equipment used in measuring the weight loss of the concrete specimen during heating is shown in fig 4. The weight change is measured with a force transducer (AB Bofors, KKM-1, 0-20N), connected with a Servogor printer. The accuracy of the transducer at ambient conditions can be estimated to $\pm 0.01 \text{ N}$ for a measured weight loss of 2 N . Under operating conditions a certain temperature increase in the transducer occurred. The increase was estimated to maximum 50°C and with a guaranteed temperature sensitivity of less than 0.01% per $^{\circ}\text{C}$ referred to the actual output voltage the error originating from this source is less than $\pm 0.01 \text{ N}$.

The specimen was suspended freely in a quartz tube, as shown in fig 4. Between the quartz tube and the transducer a spring and

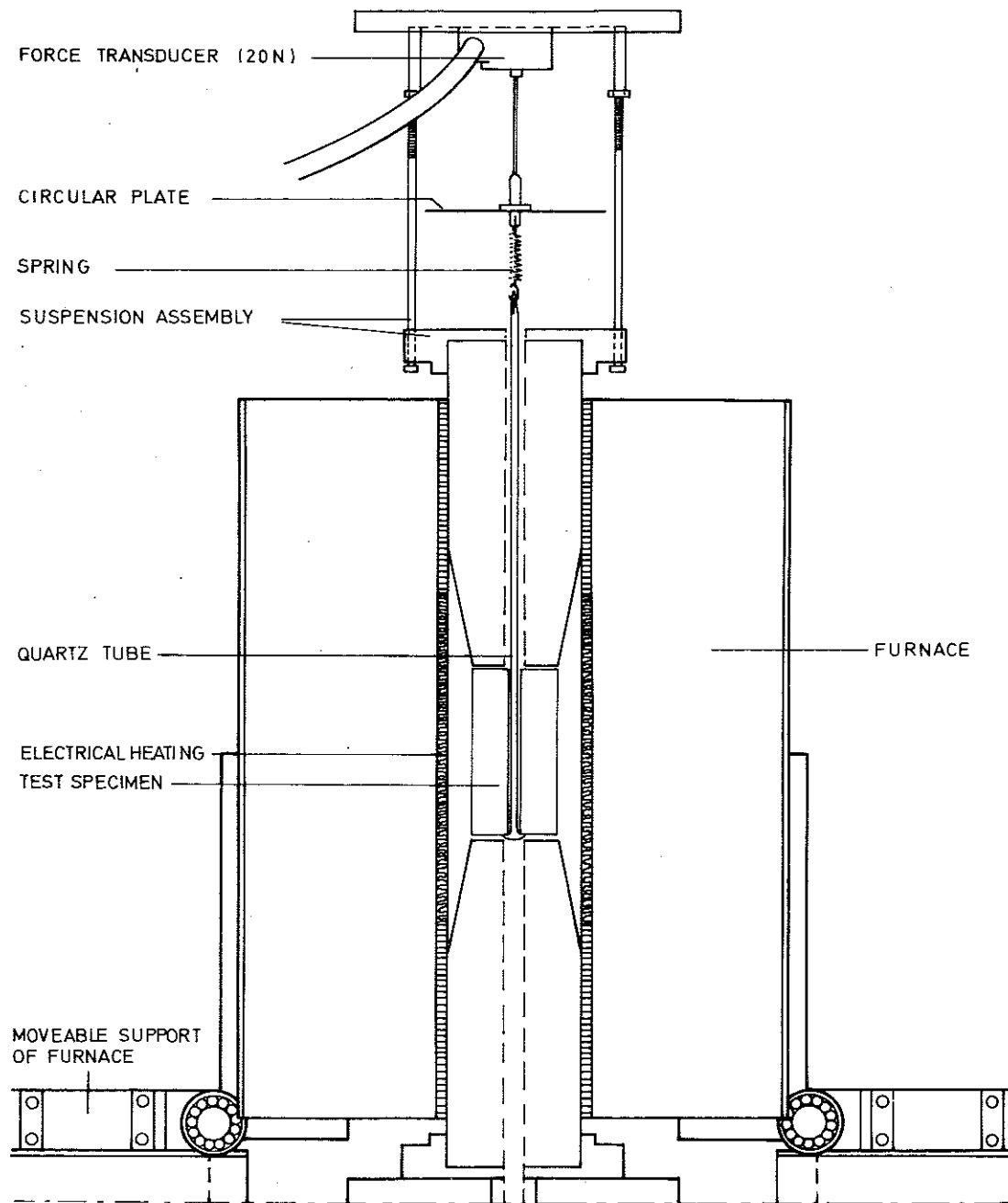


Fig 4 Equipment for weight loss measurements.

a circular plate was placed in order to prevent the transducer from a sudden unintentional overloading and from exposure of steam and heat. The plungers were placed as before in order to give similar testing conditions, though it was ensured that the specimen was hanging quite freely. The distance between the lower plunger and the bottom surface of the specimen was about 10 mm, thus allowing for the thermal expansion of the suspension system.

2.2 Specimens and materials

In choosing the size of the specimens the following considerations had to be made. On one hand the specimen should be small so as to eliminate temperature gradients. On the other hand it must be sufficiently large for ordinary concrete to be used. From such considerations the dimensions shown in fig 5 was selected. The specimen is made with a concentric hole with a diameter of 10 mm to facilitate the deformation measurements.

The specimens were cast in steel moulds, six at the time. To obtain plane and parallell surfaces at the ends of the specimen, the moulds were manufactured with high precision and the specimens were vibrated on table in a horisontal position.

The concrete was made of Standard Portland cement (Limhamn), sand from lake deposits and coarse aggregate of quartzite. The petrographic composition of the sand was dominated by quartz with some feldspar, and the quartzite rock contained 97 - 98 % quartz and 2 - 3 % feldspar. The following mix proportions were used (weight units)

Cement	1
Water	0.6
Sand (< 8 mm)	2.88
Aggregate (8 - 12 mm)	1.92

The specimens were water cured for five days and then cured in 65 % RH, 20°C up to the time of testing. Some specimens were water saturated or dried in 105°C before the test, see 2.3. The desired age at testing was set to 5 months (21 weeks), but for practical reasons a variation between 19 and 27 weeks was accepted. In one single case - where the specimen was water saturated before the test - the age

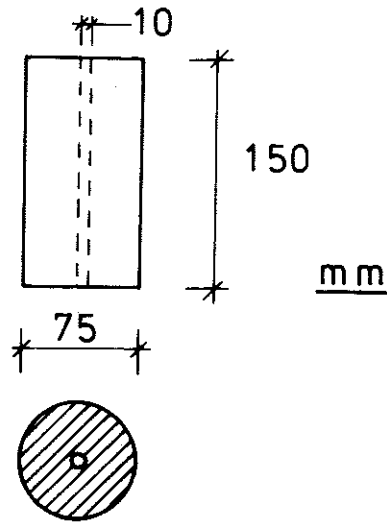


Fig 5 Dimensions of specimen.

Table 1. Thermal conductivity of the concrete at ambient conditions

TREATMENT	MEAN TEMPERATURE °C	MOISTURE CONTENT %(weight)	DENSITY kg·dm ⁻³	k W·m ⁻¹ ·°C ⁻¹
Standard cured 65% RH, 20°C	19.8	1.9	2.16	1.79
Predried in 110°C for 24 hrs	19.9	0.13	2.23	1.28
Stored in water for 96 hrs	19.9	5.5	2.29	1.86

30 weeks was accepted. The actual age of testing in each case is accounted for in tables 2 - 5.

In order to check the quality of the concrete three 150 mm cubes were cast from each batch. The compressive strengths of the cubes were determined at the age of testing. The relation between the strength of the cylindrical specimens f_{cc}^{spec} and the cube strength f_{cc}^{cube} was determined separately. When the specimens were tested in the test equipment used in the main tests the ratio $\alpha = f_{cc}^{spec} / f_{cc}^{cube}$ was determined to 0.75 as an average of 14 specimens tested. The coefficient of variation was 8.9 %. When testing the cylindrical specimens in an another testing machine between steel plates the ratio α was obtained to 0.85 as an average of 21 tests. In this case the coefficient of variation was 7.6 %. The difference between the two cases may be attributed to additional excentricity exhibited by the testing equipment. To obtain the reference strength of the specimens from the cube strength the value $\alpha = 0.75$ was used.

The coefficient of thermal conductivity k of the concrete used in the tests was determined at the Höganäs Central Laboratory. At ambient conditions k was determined under different moisture conditions as shown in table 1. In fig 6 is shown the variation of k with the temperature during heating as well as during cooling, measured by the Stålhane-Pyk method on an initially standard cured specimen. Care should be taken when interpreting the results for temperatures below 100°C, where the measurements will depend on the selected geometry of the specimen and other test conditions.

2.3 Test program

The main test program is divided into 4 main categories:

- A. The specimens were loaded to a certain stress level and then heated until failure occurred or to 800°C.
- B. The specimens were heated to a certain stabilized temperature level and then loaded to failure.

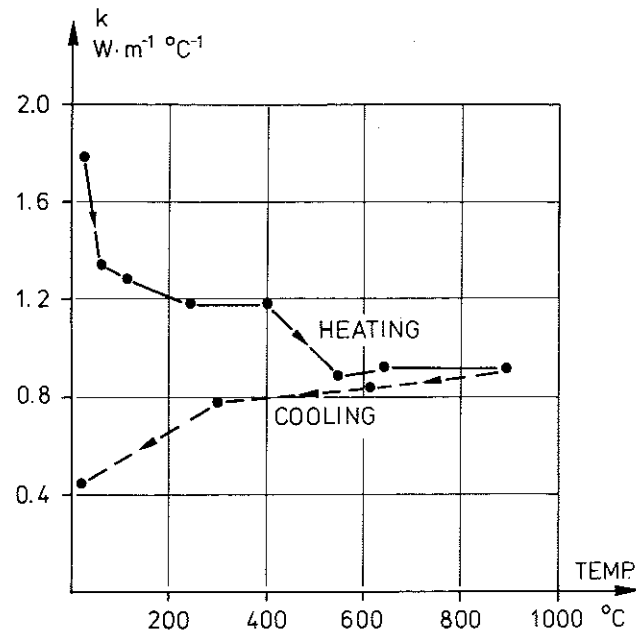


Fig 6 The variation with the temperature of the thermal conductivity k .

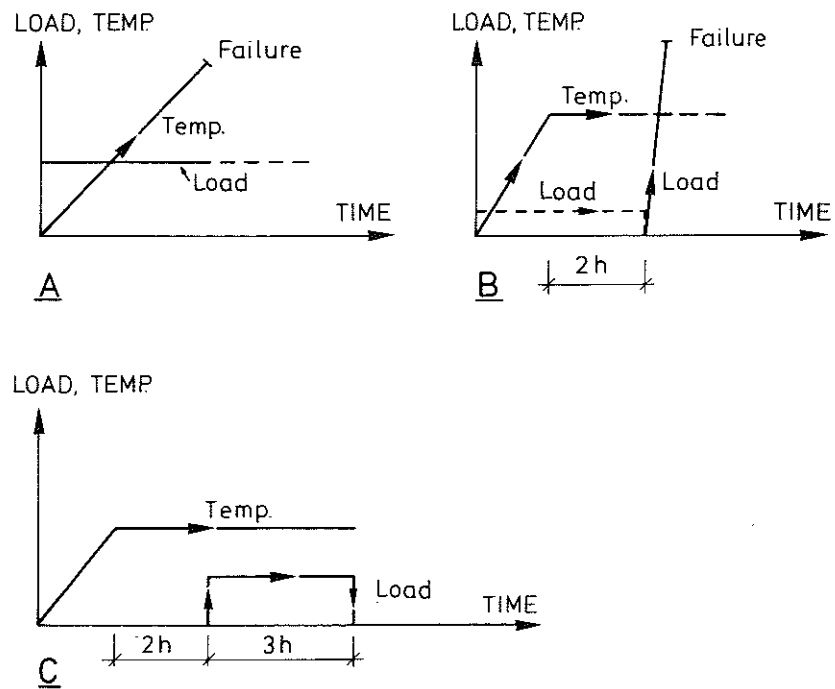


Fig 7 Load and temperature histories in the test series A, B and C.

- C. The specimens were heated to a certain stabilized temperature and then loaded. The creep under constant load was measured. The load was removed after 3 hours and the recovery was observed.
- D. Miscellaneous, including restrained deformation during heating, stepwise loading during heating and some other combinations of load and temperature histories.

The load and temperature histories of categories A - C are illustrated in fig 7.

2.3.1 Test series A

In the test series A the main parameters were

Load level (0, 22.5, 35, 45, 67.5, 90 % of the strength at 20°C)

Rate of heating (1 and 5°C · min⁻¹, maximum capacity of furnace)

Moisture conditions (Standard (STD), predried (DRY) and water saturated (SAT))

The details of the test program are compiled in table 2. The load level is given in per cent of the ambient temperature strength of the specimen, which is assumed equal to 75 % of the cube strength for respective batch, cf. 2.2. The rate of heating refers to an unprotected thermocouple attached to the surface of the specimen which is valid for all specimens. The time-temperature curve corresponding to the maximum capacity of the furnace is shown in fig 8.

Standard curing implies storing in climate chamber with 65 % RH and 20°C while "predried" refers to drying in 105°C to equilibrium. The water saturation was accomplished by vacuum pressurization. The weight-loss due to drying and the weight increase due to saturation is given in table 2 for each individual case in per cent of the dry weight. In table 2 is also given the age at testing, the cube strength and a batch identification (casting date).

Table 2. Scope of test series A

NO	STRESS %	RATE OF HEATING $^{\circ}\text{C}\cdot\text{min}^{-1}$	TREAT- MENT	WEIGHT CHANGE %	BATCH	CUBE STRENGTH MPa	AGE WEEKS
A1	0	1	STD	-	720529	64.0	22
A2a	22.5	1	STD	-	720811	55.1	23
A2b	22.5	1	STD	-	720619	58.4	26
A3	45.0	1	STD	-	720529	64.0	22
A4	67.5	1	STD	-	720619	58.4	23
A5	0	5	STD	-	720811	55.1	26
A6	22.5	5	STD	-	720619	58.4	23
A7	35.0	5	STD	-	740611	52.4	23
A8	45.0	5	STD	-	720529	64.0	23
A9	67.5	5	STD	-	720619	58.4	23
A10	90.0	5	STD	-	720612	58.7	21
A11	0	MAX	STD	-	720612	58.7	24
A12a	22.5	MAX	STD	-	720619	58.4	23
A12b	22.5	MAX	STD	-	730113	51.1	23
A13	45.0	MAX	STD	-	720612	58.7	23
A14	67.5	MAX	STD	-	720811	55.1	27
A15a	90.0	MAX	STD	-	720906	51.6	24
A15b	90.0	MAX	STD	-	730113	51.1	23
A16	0	5	DRY	-2.8	731009	46.6	19
A17	22.5	5	DRY	-2.9	731009	46.6	19
A18	45.0	5	DRY	-2.6	731009	46.6	19
A19	67.5	5	DRY	-2.6	731009	46.6	19
A20	0	5	SAT	+4.9	720518	54.3	26
A21	22.5	5	SAT	+5.5	720421	48.0	30
A22	45.0	5	SAT	+4.1	730131	50.8	21
A23	67.5	5	SAT	+4.1	730131	50.8	21

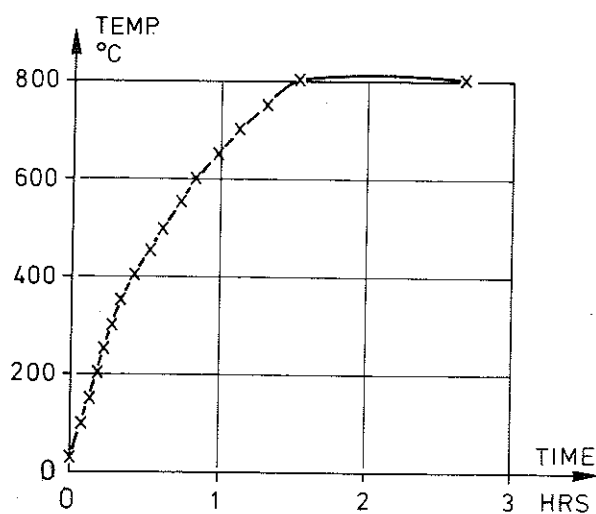


Fig 8 Time variation of furnace temperature at maximum rate of heating.

2.3.2 Test series B

The purpose of test series B is to obtain stress-strain relationships at different stabilized temperature levels. The test program is given in table 3. The main parameter in this series is the temperature level, which varied from 20 to 795°C. In table 3 is given the actual temperature in each individual test, as measured by thermocouples inside the specimens. Other parameters varied in series B were rate of heating (1 or 5°C · min⁻¹ and MAX, cf. 2.3.1) and rate of loading (0.23 and 0.057 MPa · s⁻¹). The influence of a stress applied during heating was also investigated. The applied stress is given in table 3 in % of $0.75 \cdot f_{cc}^{cube}$. This stress was removed prior to the test as indicated in fig 8. In most cases the tests were performed twice for each combination of parameters. This is indicated by letters a and b preceding the test identification numbers in table 3.

2.3.3 Test series C

Test series C comprises creep tests at constant, stabilized temperature. A constant load was applied after the actual test temperature was reached, sustained for 3 hrs and then removed. The main parameters were temperature level and stress level, the specifications for each test given in table 4. As before, the stress is given in per cent of $0.75 \cdot f_{cc}^{cube}$. The influence of the rate of heating was also studied in the tests performed at 200 and 650°C. The temperatures given in table 4 are the values measured in each individual test on thermocouples inside the specimens. In the table is also given the weight loss during the tests in per cent of the initial weight.

2.3.4 Test series D

Test series D includes tests with different loading and temperature histories. The purpose of these tests is to validate the model being developed on the basis of the tests A - C. In tests D1 - D4 the deformation was restrained throughout the tests, i.e. held equal to zero, and the load was measured. The specimen was heated at constant rate up to 800°C as shown in table 5. The same temperature treatment was used in the tests D5 - D9, where the load was applied stepwise as shown in the table. In tests D10 - D14 the temperature was increased to a certain level and then stabilized. The loading histories used are shown in the table.

Table 3. Scope of test series B

NO	TEMPERATURE	RATE OF HEATING $^{\circ}\text{C}\cdot\text{min}^{-1}$	RATE OF LOADING $\text{MPa}\cdot\text{s}^{-1}$	STRESS DURING HEATING	BATCH	CUBE STRENGTH MPa	AGE WEEKS
B1a	20	-	0.057	-	730402	51.0	19
B1b	20	-	0.057	-	730402	51.0	19
B2a	20	-	0.23	-	730326	51.3	19
B2b	20	-	0.23	-	730326	51.3	19
B2c	20	-	0.23	-	730326	51.3	19
B2d	20	-	0.23	-	730326	51.3	19
B3a	130	5	0.23	-	730312	50.0	21
B3b	130	5	0.23	-	730312	50.0	21
B4	180	1	0.23	-	730303	49.6	20
B5a	190	5	0.23	-	730219	50.0	21
B5b	180	5	0.23	-	730219	50.0	21
B6a	180	MAX	0.23	-	730303	49.6	20
B6b	170	MAX	0.23	-	730303	49.6	20
B7a	190	5	0.057	-	730312	50.0	21
B7b	205	5	0.057	-	730312	50.0	21
B8a	270	5	0.23	-	730215	53.8	22
B8b	255	5	0.23	-	730219	50.0	21
B9a	405	5	0.23	-	730219	50.0	21
B9b	400	5	0.23	-	730219	50.0	21
B10	440	5	0.23	-	740618	50.8	24
B11a	495	5	0.23	-	730205	53.2	22
B11b	505	5	0.23	-	730215	53.8	21
B12a	640	1	0.23	-	730612	54.4	24
B12b	665	1	0.23	-	730622	48.4	19
B13a	640	5	0.23	-	730205	53.2	21
B13b	650	5	0.23	-	730205	53.2	21
B14a	630	MAX	0.23	-	730215	53.8	21
B14b	670	MAX	0.23	-	730215	53.8	21
B15a	650	5	0.057	-	730604	43.5	22
B15b	640	5	0.057	-	730528	49.3	23
B16	770	5	0.23	-	730215	53.8	21
B17a	780	5	0.057	-	731113	48.4	21
B17b	795	5	0.057	-	731113	48.4	23
B18	210	5	0.23	45	740618	50.8	23
B19a	325	5	0.23	21	730604	43.5	23
B29b	340	5	0.23	17	730612	54.4	23
B20	350	5	0.23	45	730604	43.5	24
B21a	425	5	0.23	22.5	740618	50.8	23
B21b	425	5	0.23	22.5	740618	50.8	24
B22a	535	5	0.23	22.5	740618	50.8	23
B22b	535	5	0.23	22.5	740618	50.8	23
B23	640	5	0.23	10	730618	49.7	24
B24	680	5	0.23	17	730612	54.4	24

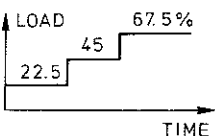
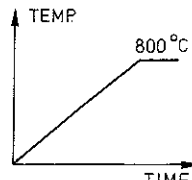
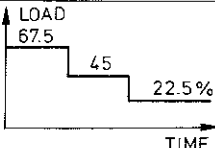
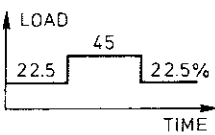
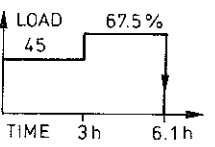
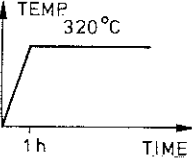
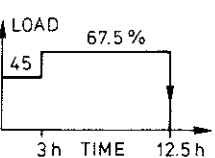
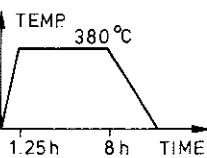
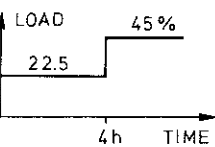
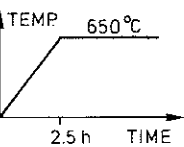
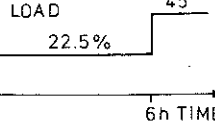
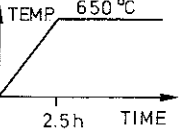
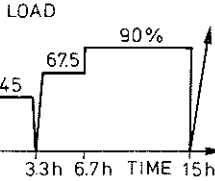
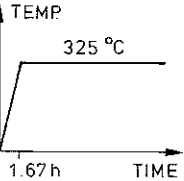
Table 4. Scope of test series C

NO	TEMPERATURE °C	STRESS %	RATE OF HEATING °C·min ⁻¹	WEIGHT LOSS %	BATCH	CUBE STRENGTH MPa	AGE WEEKS	NO- TES
C1	20	22.5	5	-	721204	56.4	22	
C2a	20	45.0	5	-	721218	42.3	21	
C2b	20	45.0	5	-	721204	56.4	22	1)
C3a	20	67.5	5	-	730103	55.8	20	
C3b	20	67.5	5	-	721218	52.3	21	1)
C4a	20	90.0	5	-	721227	51.1	20	
C4b	20	90.0	5	-	730103	55.8	20	1)
C5	125	0	5	-2.4	720923	44.2	22	
C6a	130	22.5	5	-2.5	720906	51.6	24	
C6b	130	22.5	5	-3.1	721222	52.8	21	
C7a	130	45.0	5	-2.3	720923	44.2	22	
C7b	130	45.0	5	-2.7	721227	51.1	20	
C8	120	67.5	5	-2.5	721005	48.0	23	
C9	130	90.0	5	-	720929	45.6	22	
C10	230	0	1	-3.7	721227	51.1	20	
C11	200	22.5	1	-2.4	721005	48.0	22	
C12	200	67.5	1	-3.4	721005	48.0	22	
C13a	205	0	5	-3.2	721005	48.0	22	
C13b	200	0	5	-2.6	720929	45.6	22	
C14	230	11.0	5	-	730303	49.6	21	
C15a	200	22.5	5	-3.2	720923	44.2	22	
C15b	180	22.5	5	-3.2	730113	51.1	22	
C16	190	45.0	5	-3.4	730119	51.9	22	
C17	180	67.5	5	-	730119	51.9	22	
C18	200	0	MAX	-3.6	721020	65.6	21	
C19	205	22.5	MAX	-3.3	721005	48.0	23	
C20	200	67.5	MAX	-3.2	721012	51.9	22	
C21	300	0	5	-3.7	721020	65.6	21	
C22	315	22.5	5	-3.7	721012	51.9	22	
C23	300	45.0	5	-3.5	721012	51.9	22	
C24	300	67.5	5	-	721020	65.6	23	
C25	400	0	5	-4.1	721012	51.9	22	
C26	400	22.5	5	-4.1	721012	51.9	22	
C27	400	45.0	5	-5.1	721020	65.6	23	
C28	410	67.5	5	-4.3	721020	65.6	23	
C29	500	0	5	-5.4	721020	65.6	23	
C30	485	11.0	5	-	730119	51.9	22	
C31	510	22.5	5	-5.8	721027	51.2	23	
C32	460	45.0	5	-4.8	730131	50.8	21	
C33	515	67.5	5	-	721027	51.2	24	2)
C34	640	0	1	-6.0	721204	56.4	22	
C35	650	11.0	1	-6.2	721204	56.4	22	
C36a	700	22.5	1	-	730103	55.8	21	
C36b	650	22.5	1	-5.7	730131	50.8	21	
C37	640	0	5	-6.1	721120	47.3	23	
C38	640	11.0	5	-5.7	730131	50.8	21	
C39a	660	22.5	5	-5.0	721120	47.3	23	
C39b	650	22.5	5	-5.8	731016	46.9	19	
C40	660	45.0	5	-	731120	47.3	23	2)

NO	TEMPE- RATURE °C	STRESS %	RATE OF HEATING °C·min ⁻¹	WEIGHT LOSS %	BATCH	CUBE STRENGTH MPa	AGE WEEKS	NO- TES
C41	650	0	MAX	-	721204	56.4	22	
C42	640	11.0	MAX	-	731016	46.9	19	
C43	650	22.5	MAX	-5.6	721120	47.3	23	
C44	830	0	5	-6.9	721218	52.3	22	
C45	840	11.0	5	-6.8	721204	56.4	22	
C46	790	22.5	5	-	721204	56.4	22	

- 1) Tests C2b, C3b and C4b were performed after the respective tests C1, C2a and C3a on the same specimens.
- 2) Failure occurred when the load was applied.

Table 5. Test series D

NO	RATE OF HEATING $^{\circ}\text{C}\cdot\text{min}^{-1}$	BATCH	CUBE STRENGTH MPa	AGE WEEKS	LOAD HISTORY	TEMPERATURE HISTORY
D1 D2 D3 D4	5 5 1 1	740528 740528 740528 740528	46.7 46.7 46.7 46.7	22 22 23 25	RESTRAINED DEFORMATION	
D5 D6	5 5	740605 740605	50.1 50.1	21 22		
D7 D8	5 5	740605 740605	50.1 50.1	22 22		
D9	5	740605	50.1	23		
D10	5	740611	52.4	22		
D11	5	740611	52.4	22		
D12	5	740611	52.4	22		
D13	5	740611	52.4	23		
D14	5	740605	50.1	24		

3 TEST RESULTS

3.1 Temperatures

As mentioned in 2.1.1 the temperature is measured in single points in the specimens during the tests. As an example, fig 9 shows the thermocouple readings at different locations for a specimen heated at $5^{\circ}\text{C} \cdot \text{min}^{-1}$ to 800°C .

To obtain more detailed information about the transient temperature distribution under different rates of heating and different moisture conditions a computer program was used to simulate the heat flow into the specimens. The program solves the nonlinear heat conduction equation in the axisymmetrical case. The temperature dependence of the coefficient of thermal conductivity k was chosen according to fig 7 and the enthalpy i_v used in the calculations is shown in fig 10 as a function of temperature. The enthalpy curve is based on measurements of specific heat by Ödeen-Nordström /8/ and is modified in the range $100 - 200^{\circ}\text{C}$ to take into account the latent heat inherent in the evaporation of the free moisture. The curve is also modified in the range $530 - 550^{\circ}\text{C}$ accounting for the endothermic dehydration of $\text{Ca}(\text{OH})_2$. The enthalpy curve thus depends on the initial moisture content as shown in fig 10.

The heat transfer conditions at the heated surface and in the center hole could be estimated so as to give good agreement with the measured temperatures near the surfaces. A comparison between measured and calculated temperatures is shown in fig 11. The curves shown in the figure are typical for the reliability of the theoretical calculations.

The program was used to calculate the temperature distributions under different rates of heating, and different moisture contents. The results are shown in fig 12 for heating at constant rates up to 800°C . Except for the maximum rate of heating the temperature gradients are moderate, and for $1^{\circ}\text{C} \cdot \text{min}^{-1}$ the temperature distribution is close to uniform.

3.2 Weight loss

In fig 13a is shown the weight loss vs. time for standard cured specimens heated at $5^{\circ}\text{C} \cdot \text{min}^{-1}$ to different maximum levels. The weight loss

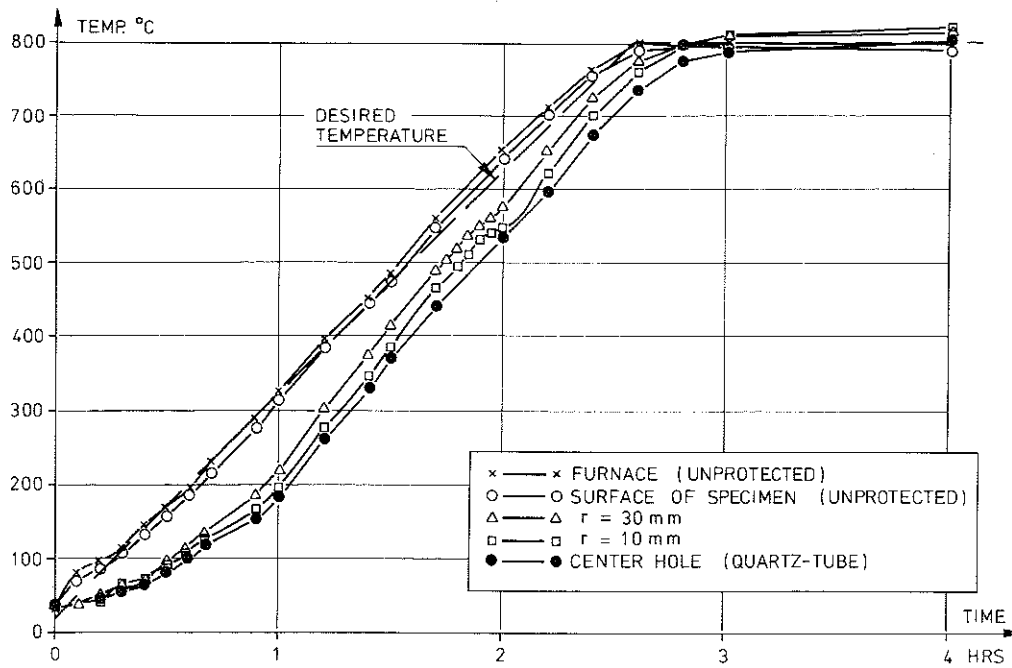


Fig 9 Measured temperatures in a standard cured specimen heated at $5^{\circ}\text{C} \cdot \text{min}^{-1}$. Age: 20 weeks.

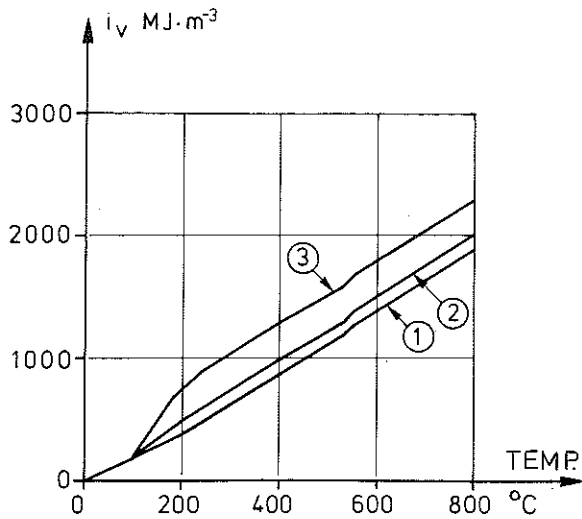


Fig 10 Enthalpy vs. temperature used in the calculations of transient heat flow into the specimens.
 Curve 1: Predried concrete (105°C).
 Curve 2: Standard cured concrete.
 Curve 3: Water saturated concrete.

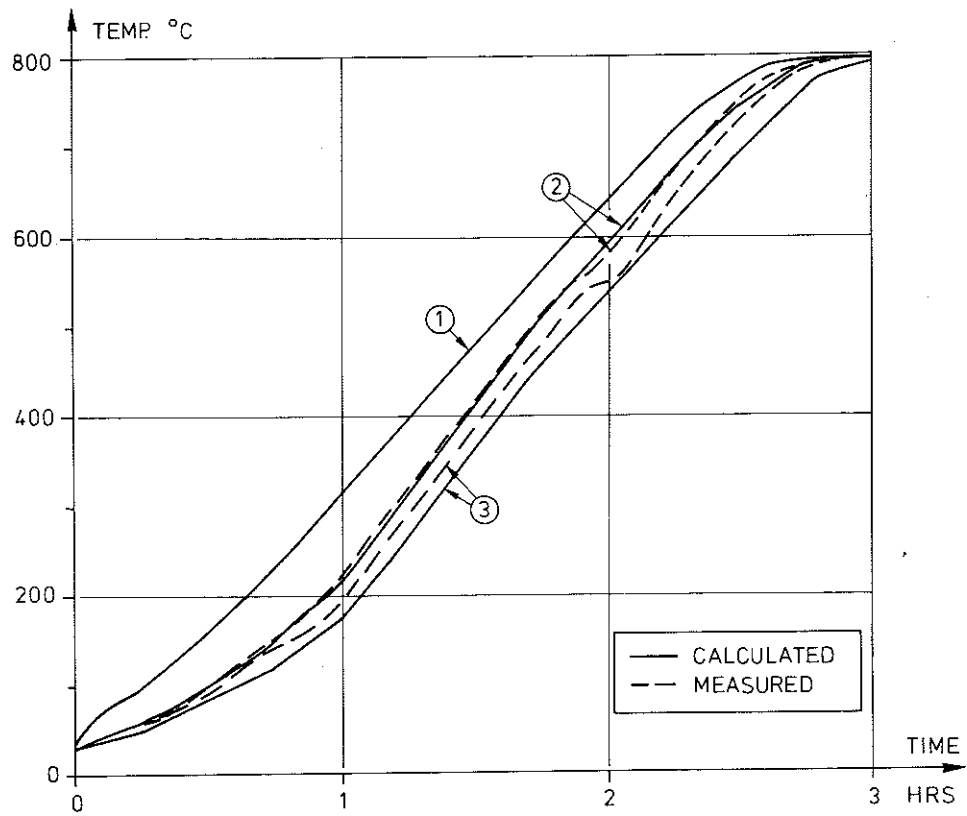


Fig 11 Measured and calculated temperatures in standard cured specimen heated at $5^{\circ}\text{C} \cdot \text{min}^{-1}$.
1. Furnace temperature (used as input).
2. Temperature in $r = 30\text{ mm}$.
3. Temperature in $r = 10\text{ mm}$.
 r = distance from centre.

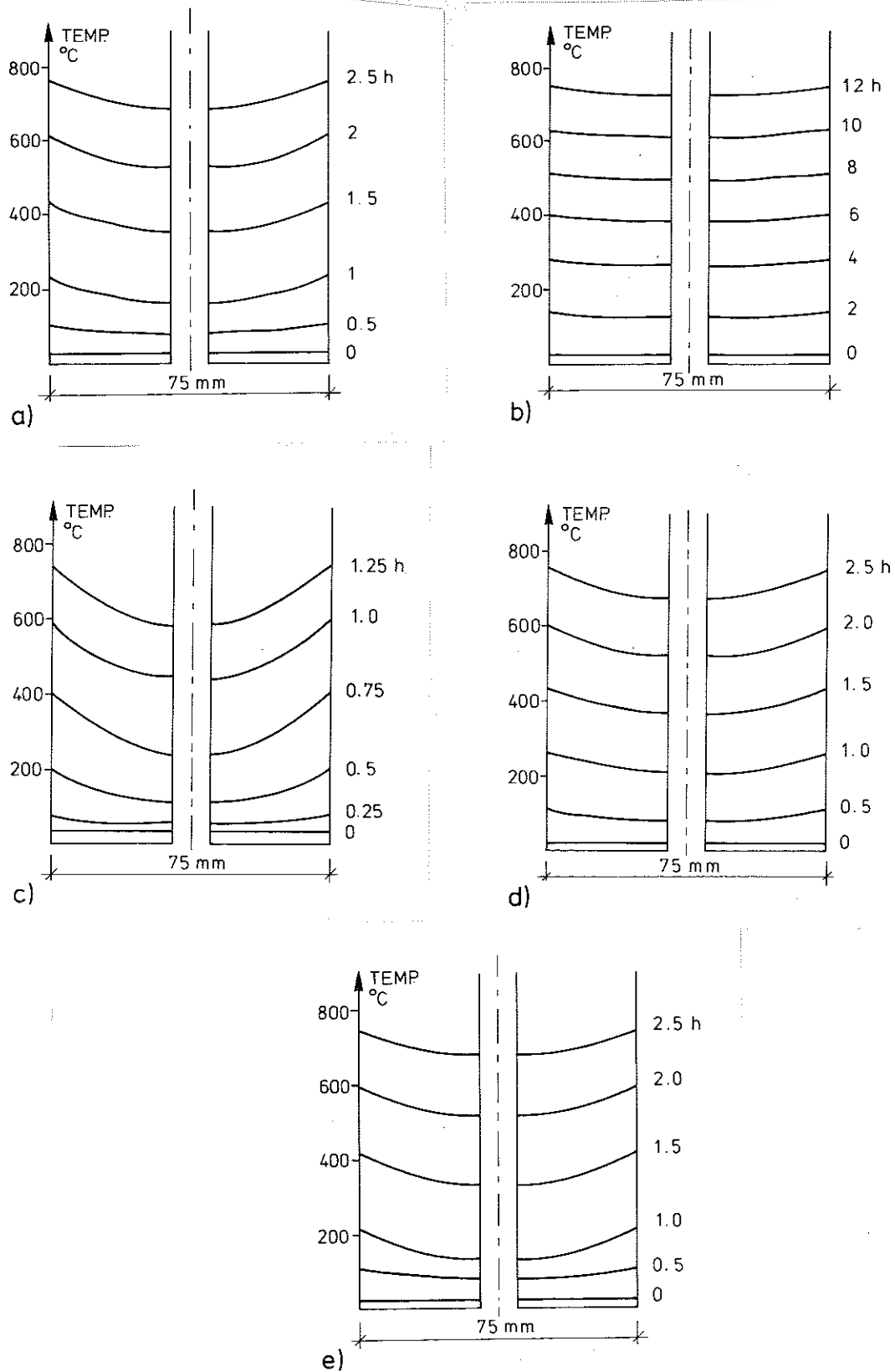


Fig 12 Calculated temperature distributions in the specimen during heating to 800°C.

- a) 5°C · min⁻¹, standard cured
- b) 1°C · min⁻¹, standard cured
- c) Maximum rate of heating, standard cured.
- d) 5°C · min⁻¹, predried.
- e) 5°C · min⁻¹, saturated.

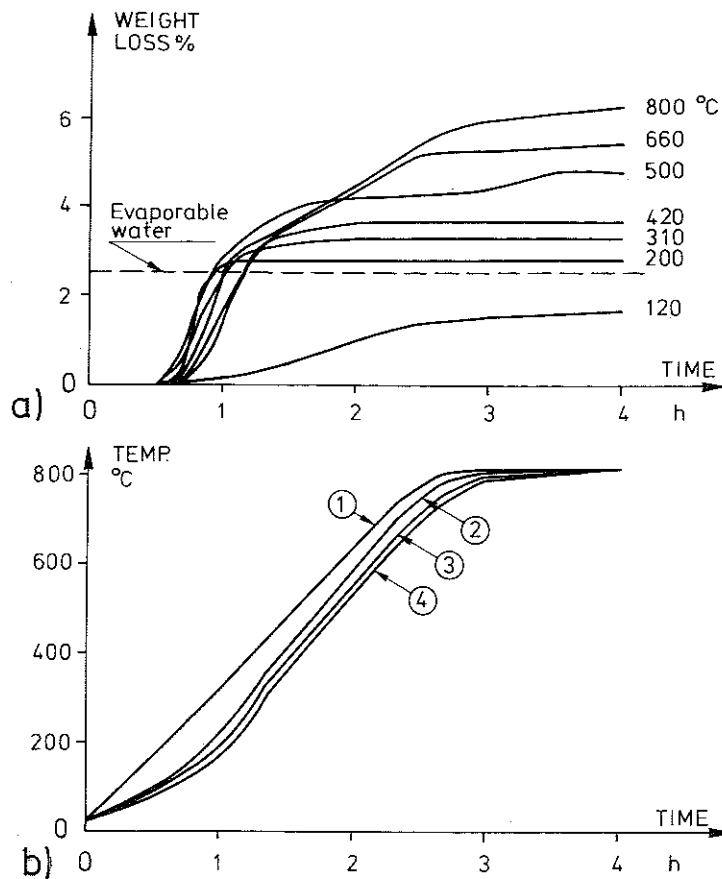


Fig 13 a) Weight loss as a function of time when the specimens are heated at $5^{\circ}\text{C} \cdot \text{min}^{-1}$ to different temperature levels. The dashed horizontal line indicates the evaporable water content determined by drying at 105°C . Age of specimens: 24-26 weeks.
 b) Temperature development in the specimens heated to 800°C .
 1. Furnace temperature.
 2. Temperature in $r = 32\text{ mm}$
 3. Temperature in $r = 22\text{ mm}$
 4. Temperature in $r = 11\text{ mm}$
 r = distance from centre of specimen.

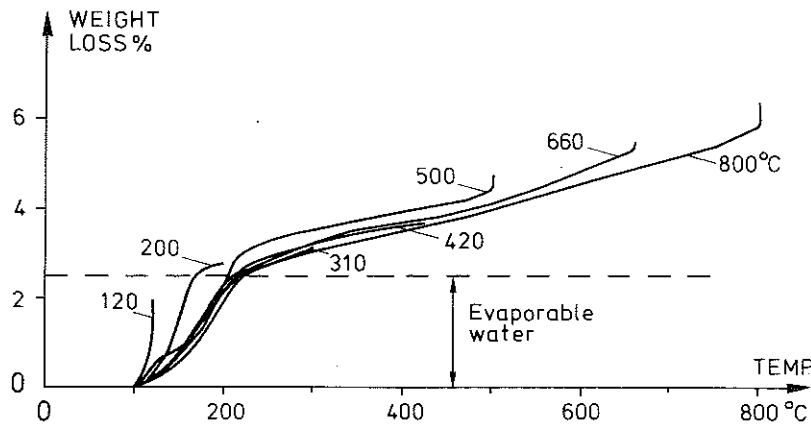


Fig 14 Weight loss as a function of the temperature at a distance 26 mm from the centre of the specimen.

is given in % of the original weight. In the figure is indicated the weight loss obtained after drying in 105°C to equilibrium. The weighing equipment did not permit measurements of temperatures inside the specimens in these tests, and detailed information of the temperature development in each single test is therefore not available. In fig 13b, however, are shown calculated temperatures for heating to 800°C to give an impression of the temperature development during the tests. It can be seen that the most rapid loss of weight is exhibited below 200°C when the evaporable moisture disappears. Above 200°C the moisture loss continues at a lower rate and after the temperature is stabilized it stops almost immediately. An exception is the curve for 120°C , where the evaporation of moisture continues at a rather high rate after the temperature is stabilized. Also when the temperature is stabilized at 500°C a continued dehydration can be discerned, probably as a result of the degradation of $\text{Ca}(\text{OH})_2$ at this level.

In fig 14, the weight loss for the tests shown in fig 13a has been plotted against the temperature in the specimen at a distance of 26 mm (0.7 R) from the centre. This temperature was estimated from the measured furnace temperature with the aid of the calculated temperature distributions shown in fig 12a. Although this estimate is uncertain it can to some extent eliminate the individual differences of the temperature exposure between the tests. Fig 14 shows that the moisture loss is a function of temperature and is virtually independent of the temperature program if the specimen is heated above 200°C . The curves also show a marked change in the rate of moisture loss when the evaporable moisture has disappeared.

In fig 15 the weight loss is plotted against temperature (26 mm from the center) for different rates of heating up to 650°C . Again it is shown that the moisture loss is related to the temperature level and that it is almost independent of the rate of heating.

Fig 16 shows the influence of the initial moisture content on the weight loss under heating ($5^{\circ}\text{C} \cdot \text{min}^{-1}$) to 800°C , the weight loss being related to the moisture content of the standard cured specimen. Although the curves start from different moisture levels the conditions are similar above 200°C , when the evaporable moisture has disappeared.

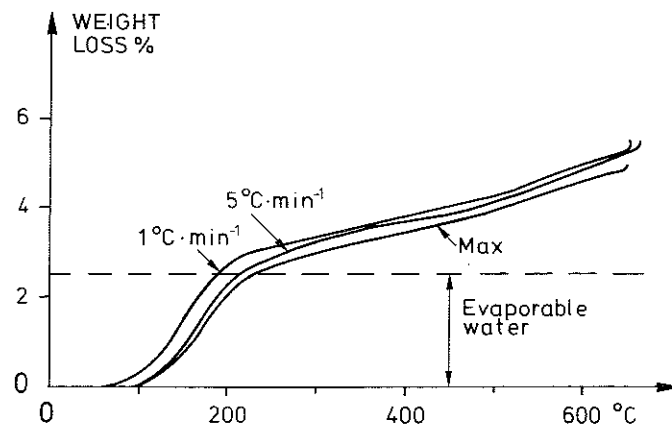


Fig 15 Weight loss as a function of temperature ($r = 26$ mm) at different rates of heating to 650° C.

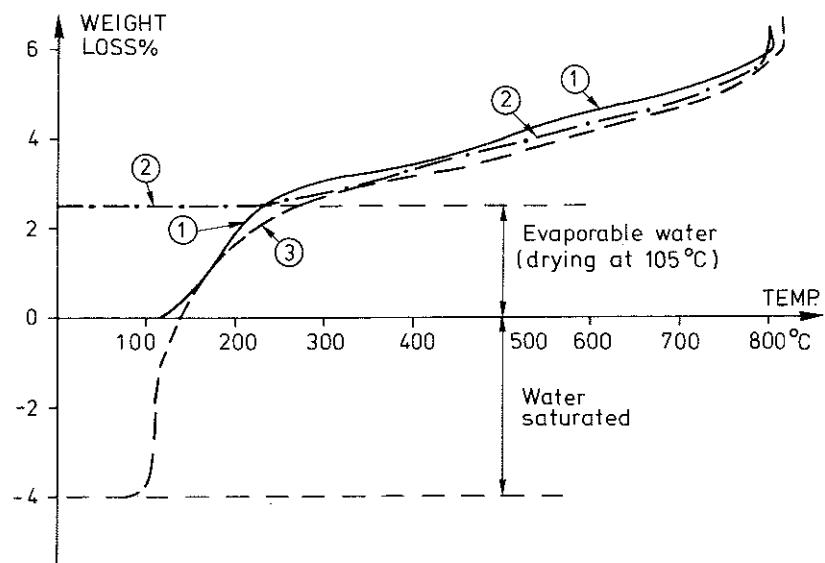


Fig 16 Weight loss as a function of temperature ($r = 26$ mm) for different initial moisture contents. Rate of heating 5° C · min⁻¹.

The conclusions from these tests are that for the small unsealed specimens in question the evaporable water has almost completely disappeared when the temperature reaches 200°C , that above this level the dehydration is mainly determined by the temperature level and is practically independent of time. It should be pointed out that for concrete in structures of larger dimension these results are not applicable. Particularly the behaviour of the evaporable water depends very much on the transport mechanisms and hence on the geometry.

3.3 Heating to failure under constant stress (test series A)

In these tests a constant compressive stress was applied initially and sustained while the specimen was heated until failure occurred. The stress level will be referred to in per cent of the strength at ambient conditions as discussed in 2.2.

The fact that the temperature is varying over the cross-section during heating makes it difficult to specify the temperature. In the results presented below the temperature of the specimen is defined as the temperature at a distance $0.7 \cdot R$ ($= 26 \text{ mm}$) from the centre, where R is the outer radius of the cross-section. This distance corresponds to the location of the centroid of a uniform stress distribution over any small sector of the circular cross section.

Fig 17 shows the results from standard cured specimens heated at $5^{\circ}\text{C} \cdot \text{min}^{-1}$ under different sustained stress levels. The deformations shown in the figure does not include the strains obtained upon initial loading. The thermal expansion is strongly reduced under stress and for a stress equal to about 40 % the thermal expansion is fully compensated by the stress-induced deformation. As the temperature approaches a critical value the compressive strain increases rapidly and ultimately failure occurs. It should be noted that the curve corresponding to 90 % stress is very uncertain due to possible divergence between the real strength of the very test specimen and the characteristic strength used. Furthermore the strength of concrete is varying very little in the temperature range between 20 and 400°C , see 3.4.

Otherwise the results shown in fig 17 agree qualitatively with results published in the literature /9, 10/. The results obtained by Schneider /10/

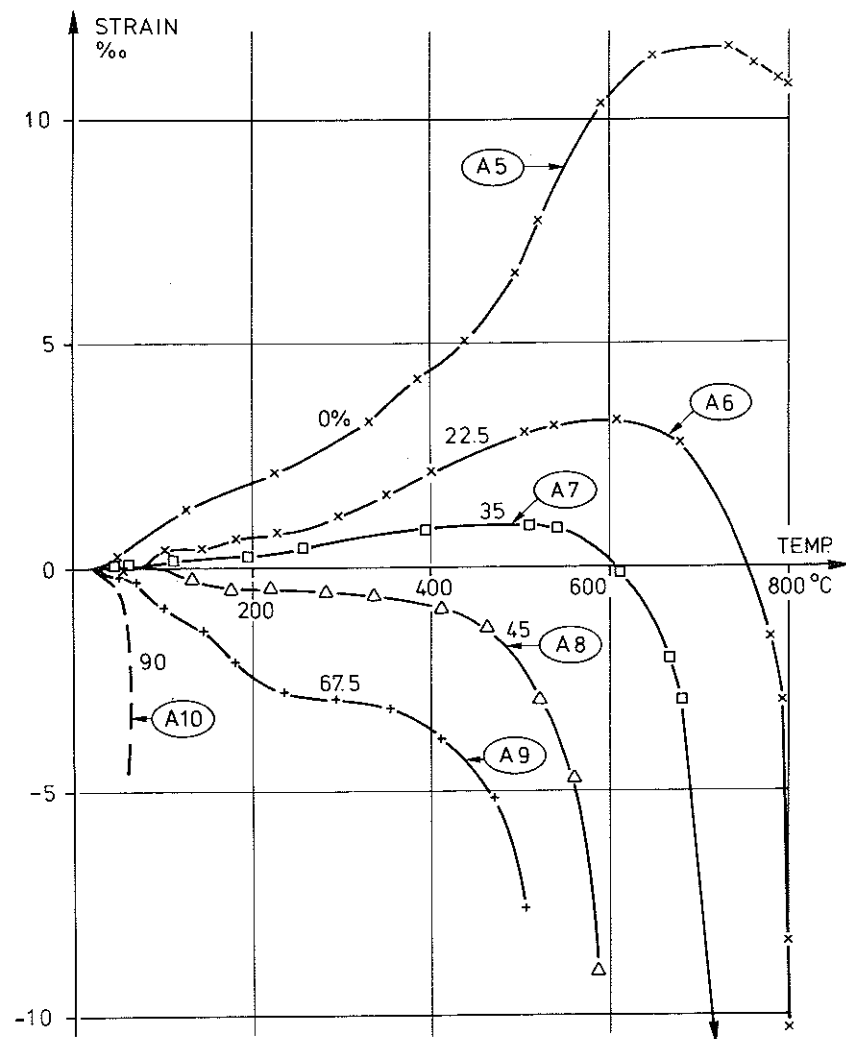


Fig 17 Deformations upon heating ($5^{\circ} \text{C} \cdot \text{min}^{-1}$) under different load levels.

show generally higher expansivity, probably due to the fact that a concrete containing more aggregate was used.

The influence of the rate of heating is shown in fig 18. The difference between specimens heated at $1^{\circ}\text{C} \cdot \text{min}^{-1}$ and $5^{\circ}\text{C} \cdot \text{min}^{-1}$ is rather small at all load levels, although at the load level 45 % the critical temperature differs about 40°C . The influence of rate of heating on the critical temperature for the load levels 45 and 67.5 % agrees well with results obtained by Schneider /10/ in similar tests with a variation in the rate of heating from 0.5 to $6^{\circ}\text{C} \cdot \text{min}^{-1}$. For the maximum rate of heating (see 2.3.1) the thermal expansion above 600°C is considerably greater than at the lower rates of heating. The deformations under load at the maximum rate of heating are similar to those at lower rates for the load levels 22.5 % and 67.5 %, while for 45 % a great difference is obtained. The critical temperature for the latter load level is 725°C for the maximum rate of heating compared with 590°C for $5^{\circ}\text{C} \cdot \text{min}^{-1}$. The strong influence of the rate of heating at this particular load level is difficult to explain. One reason may be the time dependence of the dehydration process, which has a decisive influence on the concrete strength in the range between 450 and 600°C . Another possible reason is the difference in temperature gradients which may affect the stress distribution at failure. The latter will be further discussed in chapter 5.

In the tests shown in figs 17 and 18 the temperature rise was limited to 800°C , and the specimens loaded to 22.5 % either did not fail at all (A2) or failed after the temperature was stabilized at 800°C (A6 and A12a). It is therefore inexact to state that the critical temperature for 22.5 % load is 800°C , even if it is near the truth.

Fig 19 shows the influence of the initial moisture content on the deformations under transient conditions. The predried specimens generally show higher critical temperatures, probably due to increased strength following the drying process. (The applied load is related to

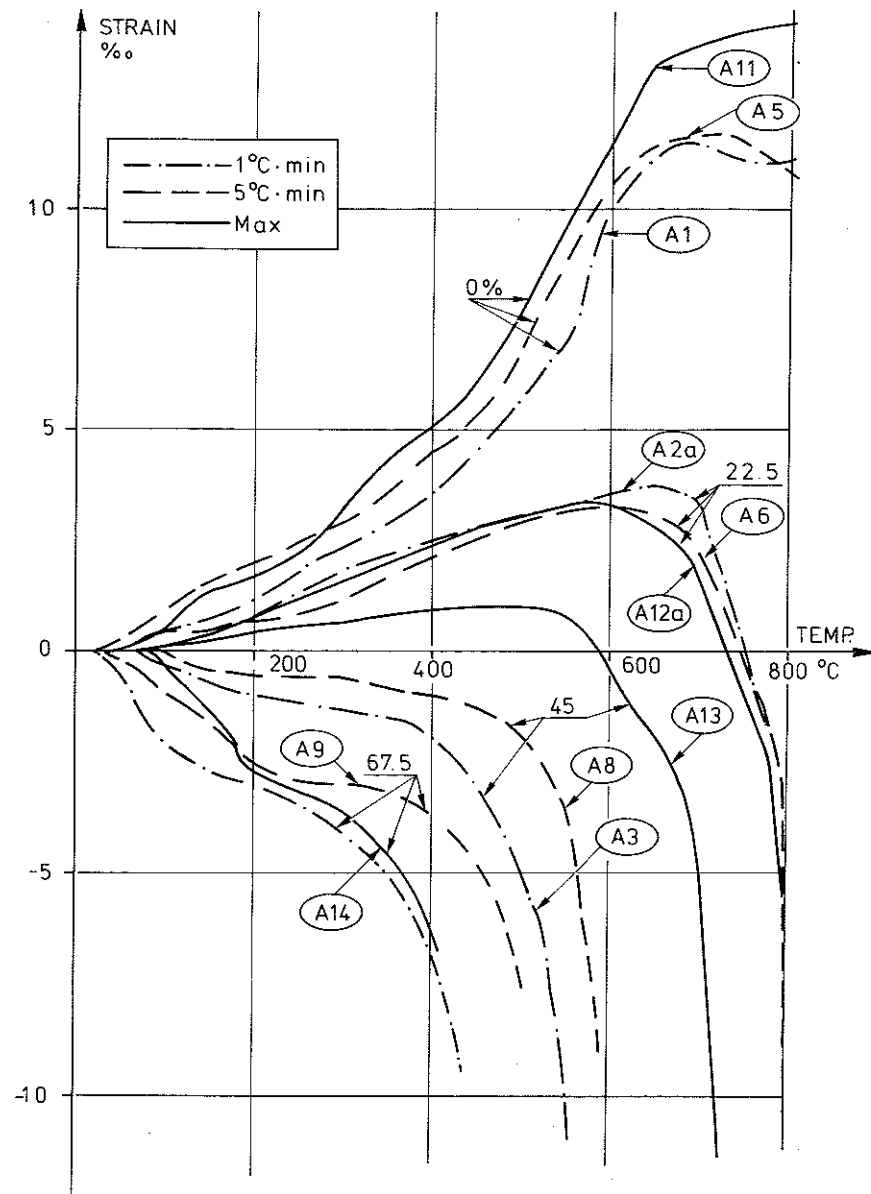


Fig 18 Influence of rate of heating on the deformations under sustained load.

standard cured cubes). The predried specimens at 45 and 67.5 % load are also less liable to deformations in the compressive direction under load. An exception is the specimen loaded at 22.5 %, where no significant difference can be seen. The results in fig 19 are as a whole difficult to explain. The influence of water saturation is not very significant, except for the free thermal expansion, which is remarkably smaller for the water saturated specimen.

In general, care should be taken when drawing conclusions for the tests shown in figs 17-19. The stress percentages assigned to the specimens may not be comparable due to the scatter in strength between specimens.

3.4 Stress-strain relations at high temperatures

Fig 20 gives a visual impression of the stress-strain relations as affected by temperature for standard cured specimens without any load during heating. The rate of loading was $14 \text{ MPa} \cdot \text{min}^{-1}$, i.e. a loading of short duration, implying that the creep can be neglected. The curves shown are mean values of two tests (for 440°C only one test was made) at each temperature level, the stress being expressed in percent of ultimate stress at 20°C given as $0.75 \times f_{cc}^{\text{cube}}$. At 20°C the ultimate compressive strength is related to the value obtained from each individual test and the curve represents an average of the four tests B2a-d. In some cases the actual temperature upon testing differs slightly between tests intended to be identical, cf. table 3. The temperature indicated on the average curves in fig 20 is then given as the mean value between the testing temperatures of the two individual tests. The variations between identical tests were negligible for temperatures above 300°C , but at lower temperatures some scatter was observed. This variation is illustrated in figs 21, 22 and 24.

The tests were performed with controlled load, which means that the specimen is crushed when the ultimate stress is obtained and the descending branch of the stress-strain curve is not recorded.

The curves in fig 20 show that with increasing temperature the ultimate stress decreases and the ultimate strain increases. For a

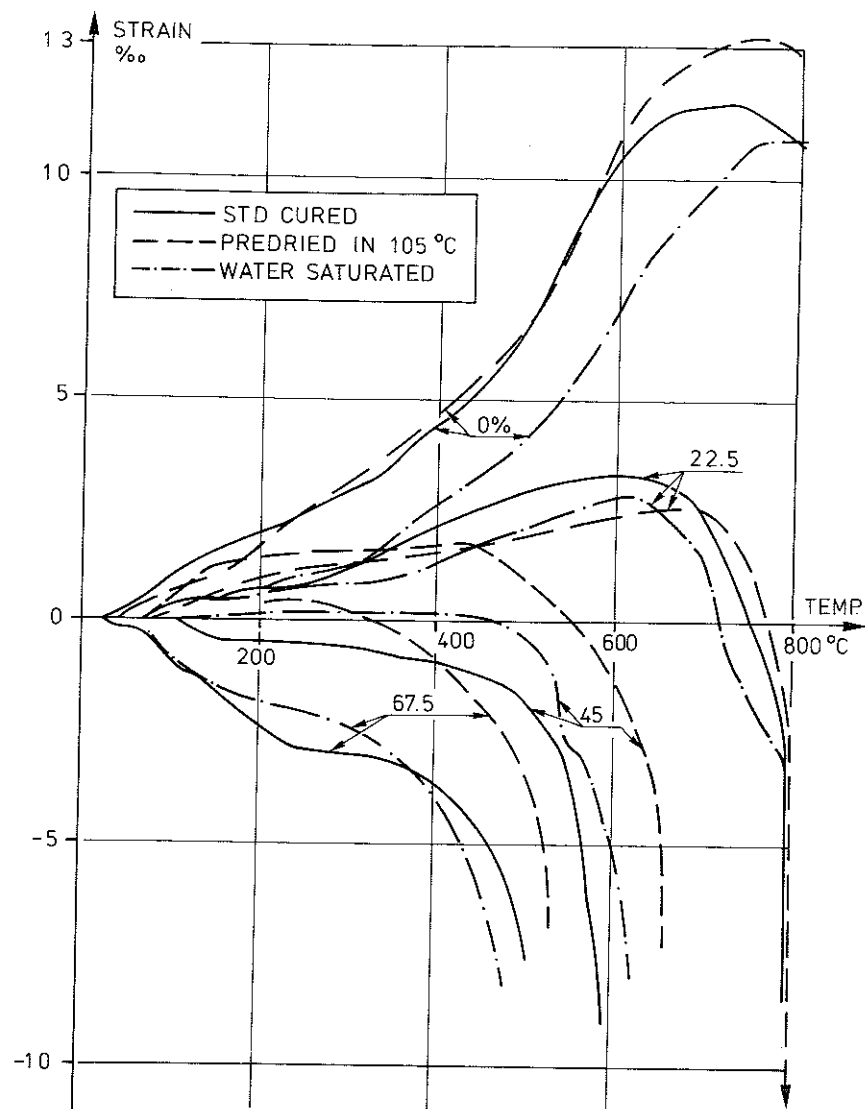


Fig 19 Influence of pretreatment on the deformations under sustained load.

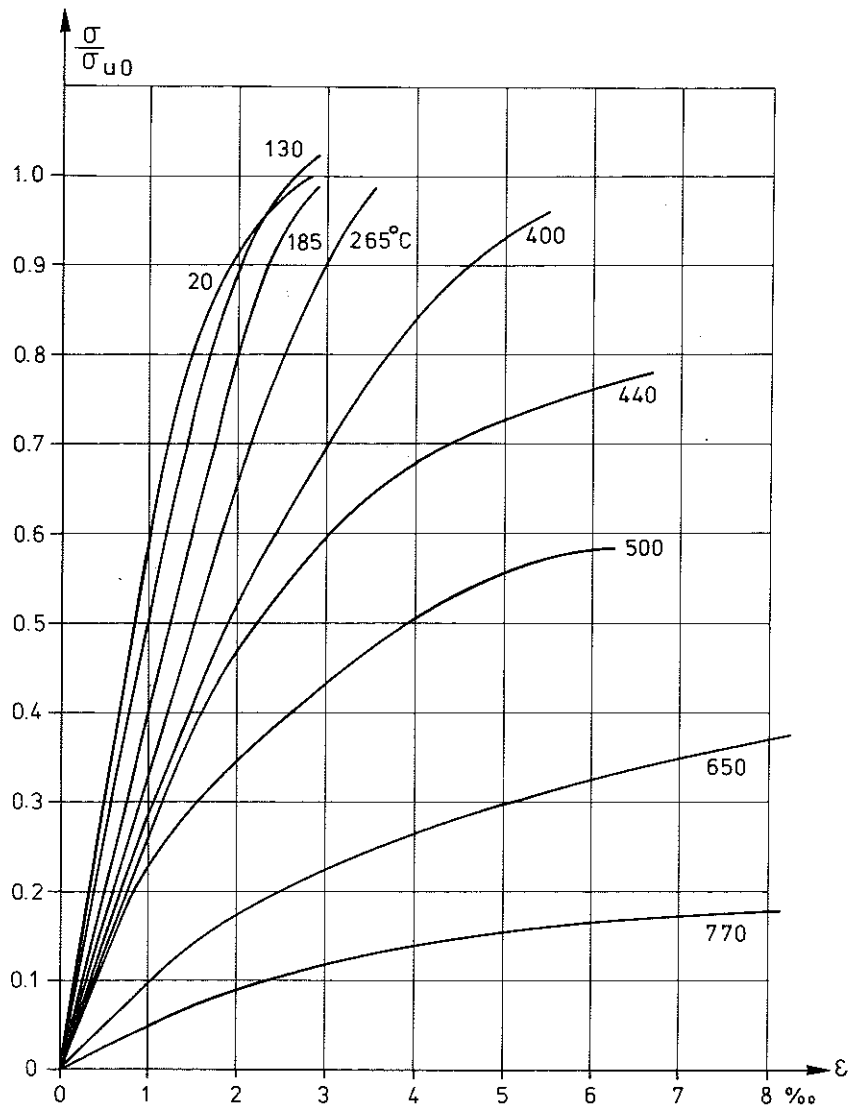


Fig 20 Stress-strain relations for different temperatures.

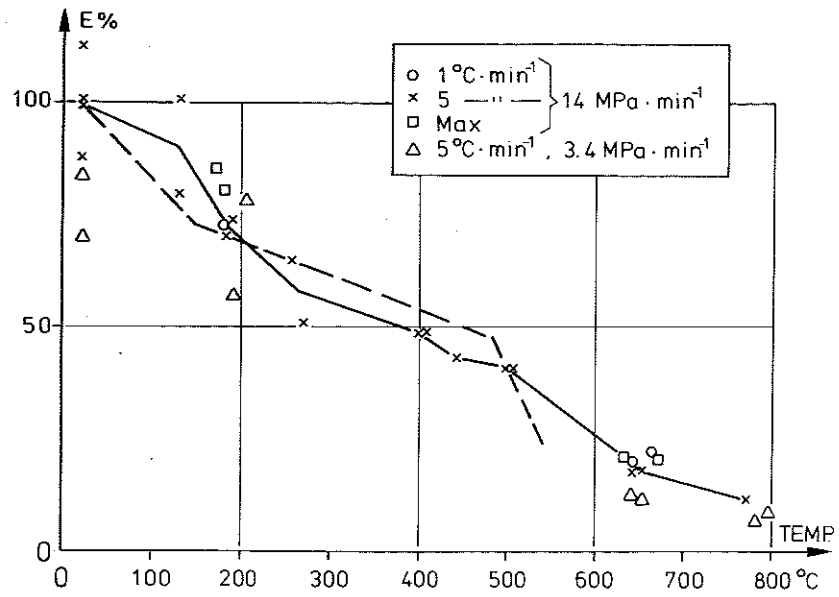


Fig 21 Effect of temperature on static elastic modulus obtained by the authors (full line) compared with dynamic modulus from Cruz /10/ (dashed line).

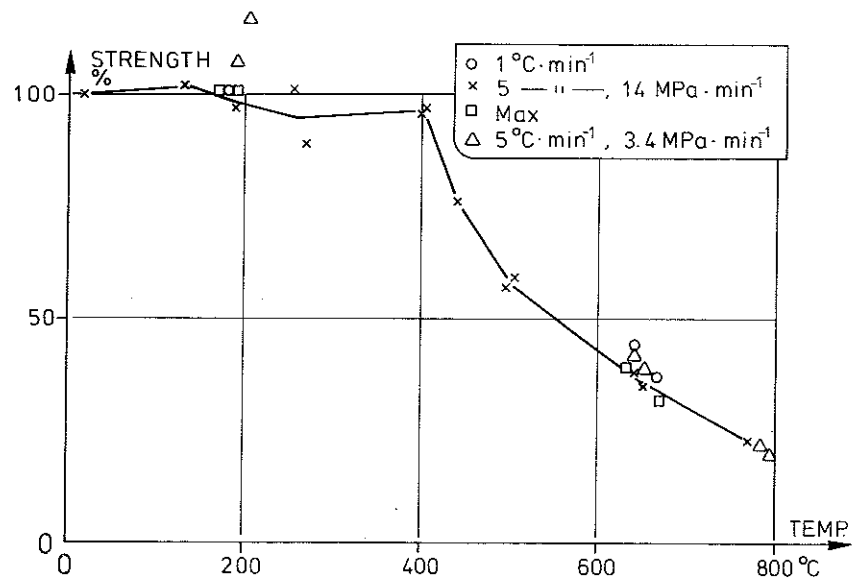


Fig 22 Effect of temperatures on the compressive strength obtained from test series B.

given stress-strain curve three characteristic parameters can be defined, the elastic modulus, the ultimate compressive strength and the ultimate strain, respectively. The influence of temperature on these parameters is shown in figs 21-23.

Fig 21 shows the effect of temperature on the elastic modulus estimated from the slope of the measured stress-strain diagrams between zero and 30 % of the ultimate stress at each temperature. The absolute value of the elastic modulus at 20°C corresponding to 100 % in fig 21 is $2.15 \cdot 10^4$ MPa obtained as an average of tests B2a-d. The full line curve in the figure refers to the average values of the elastic modulus at each temperature level. In the figure is also given a curve for the dynamic modulus obtained by Cruz /12/ for concrete with similar properties. This curve agrees well with the results obtained in the present study.

Fig 22 shows the compressive strength as a function of temperature. The compressive strength is given in percent of the ultimate stress at 20°C, defined as $0.75 \cdot f_{cc}^{cube}$. The full line curve refers to the average values for the specimens heated at $5^\circ\text{C} \cdot \text{min}^{-1}$ and loaded with $14 \text{ MPa} \cdot \text{min}^{-1}$. The strength is not affected significantly upon heating to 400°C, but above this value it is decreasing rapidly.

In fig 23 the curve from fig 22 (full line) is compared with the failure temperature obtained from series A, for specimens heated to failure under sustained load. The points corresponding to standard cured specimens heated to 1 and $5^\circ\text{C} \cdot \text{min}^{-1}$ respectively generally fall near the curve and the same applies to the saturated specimens. For the predried specimens the strength is somewhat higher probably due to increased hardening during the drying process. For specimens heated at "maximum rate" the picture is contradictory, which probably is explained by the high temperature gradients present during the heating. The general conclusion is, however, that the combination of stress and temperature at failure is virtually the same whether the concrete is loaded to failure at stabilized temperature or if it is heated to failure under sustained stress.

In fig 23 are also reproduced results from Schneider /10/ on specimens heated to failure under sustained load (broken line). Although

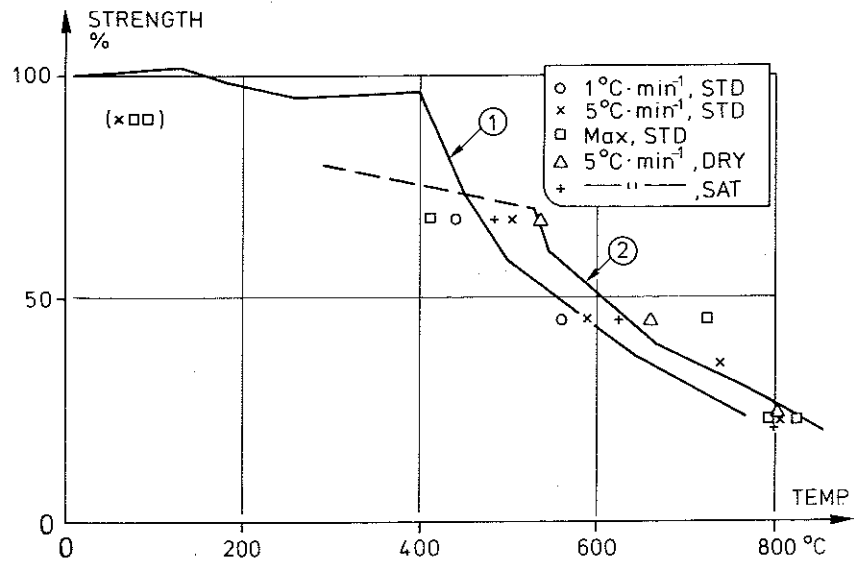


Fig 23 Compressive strength vs. temperature. The single points represent data obtained by the authors for specimens heated to failure under sustained load (Test series A). Curve 1: Specimens loaded to failure at stabilized temperatures, from fig 22. Curve 2: Specimens heated to failure under sustained load, from /8/, rate of heating $2^{\circ}\text{C} \cdot \text{min}^{-1}$.

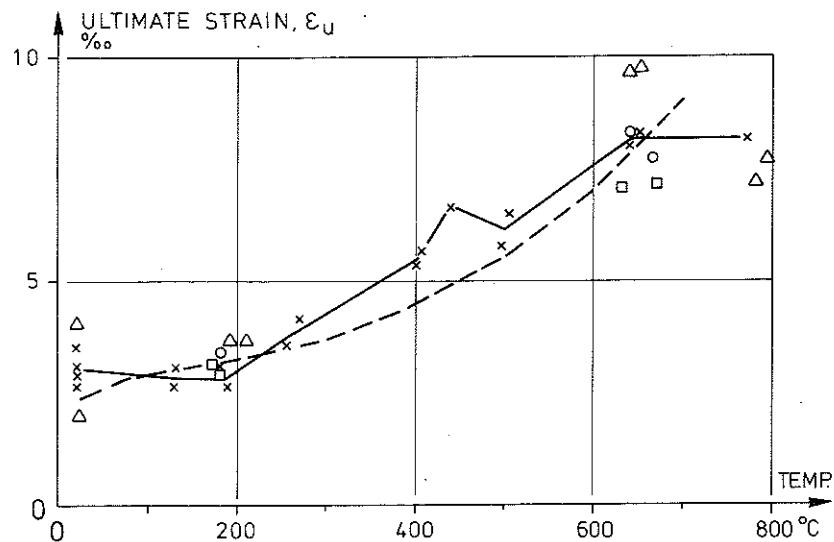


Fig 24 Effect of temperature on the ultimate strain, measured on specimens unstressed while heated. The full line indicates average values from series B and the dashed line tests from Furamura /11/.

this curve corresponds to concrete with different composition, (Portland cement, quartztype aggregate, ratio 1:5.4, $w/c = 0.54$), it generally confirms the conclusions made above.

The third parameter characterising the stress strain curve is the ultimate strain, ϵ_u (strain at ultimate stress). Its variation with the temperature is shown in fig 24, and compared with results obtained by Harada /13/. The results agree well with each other despite the fact that Harada's tests were performed under deformation control.

The points in figs 21, 22 and 24 include a limited number of tests where the specimens were heated at $1^\circ\text{C}\cdot\text{min}^{-1}$ and maximum rate respectively. These tests do not indicate any significant influence of the rate of heating on the stress-strain relation. The same figures also include some tests performed with a lower rate of loading ($3.4 \text{ MPa}\cdot\text{min}^{-1}$). A lower rate of loading should tend to increase the deformations, but this is not quite obvious from the results shown.

The results shown hitherto refer to specimens heated without stress. It is known from the literature, see for instance /9/, that specimens being stressed under heating obtain higher strengths and lower deformabilities when tested at high temperatures. The tests B18-B24 in the present investigation were performed in order to study this influence. The results from these tests are compiled in fig 25, for elastic modulus (25a), compressive strength (25b) and ultimate strain (25c). In the figures are also shown the corresponding average curves for unloaded specimens taken from figs 21, 22 and 24. In spite of the scatter in these data it is clear that the deformability is considerably affected by the presence of load during heating. The elastic modulus increases and the ultimate strain decreases markedly. The effect on the strength is not significant, even if a slight increase is obtained in single cases.

3.5 Creep at constant temperature

In test series C the creep under sustained load at constant temperature was measured. For each temperature level unloaded companion specimens were tested to obtain the volume change (e.g. shrinkage)

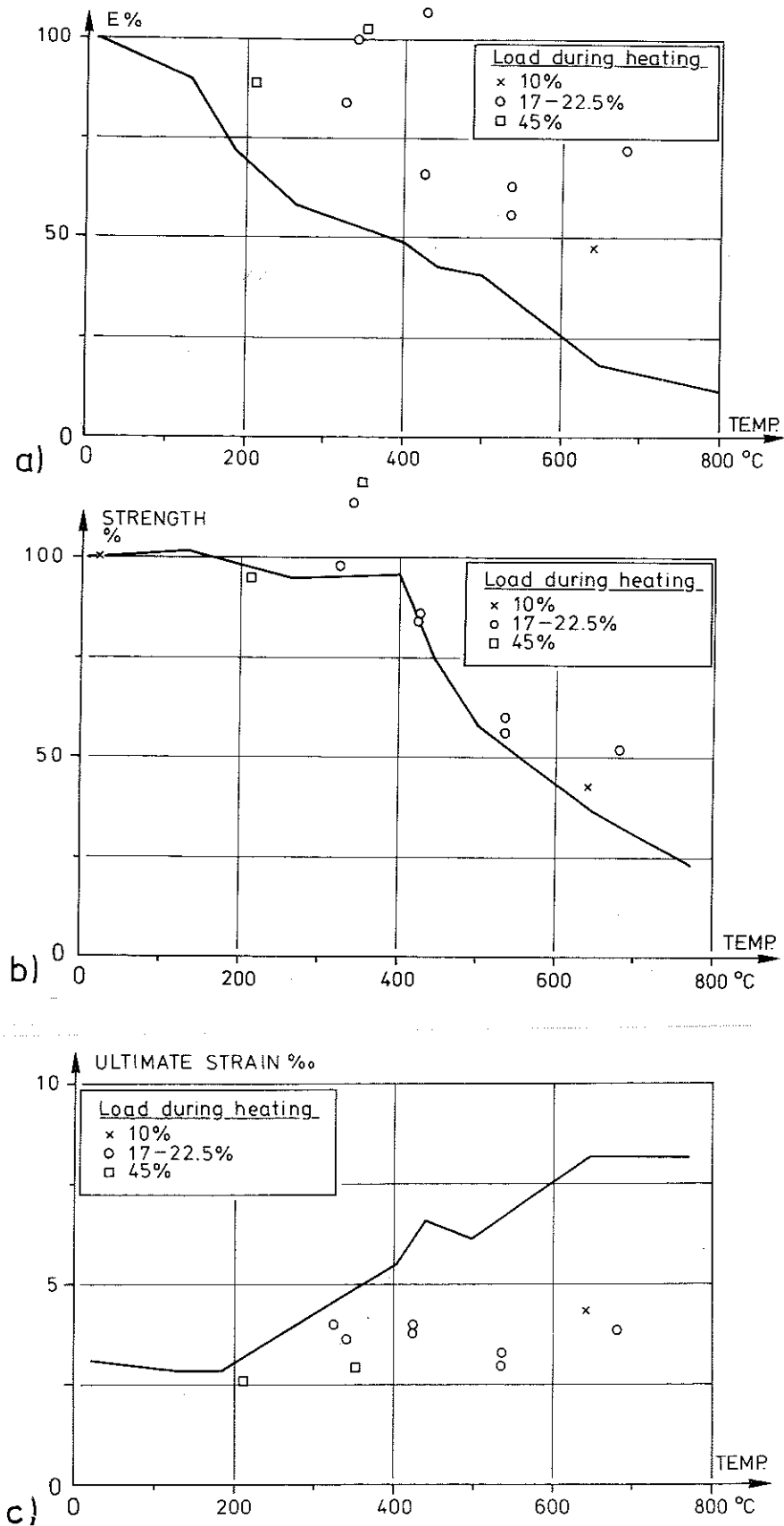


Fig 25 Elastic modulus (a), strength (b) and ultimate strain (c) as functions of temperature for specimens stressed while heated (single points). The full lines indicate the results from specimens unstressed during heating (figs 21,22 and 24).

at constant temperature. No measurable deformations on these specimens were observed during the time period corresponding to the creep tests (3 hrs). This was valid for all temperature levels tested without exception and accordingly no corrections had to be made on the measured deformations under load.

The complete course of events is shown for a typical test in series C in fig 26 (curve 1). The specimen is heated to 400°C while the thermal expansion develops. The load is applied after the temperature is stabilized, sustained during three hours and then removed again. The test is terminated by cooling the specimen, which gives rise to a decrease in strain.

As shown in the figure the time-dependent creep strain under sustained load and temperature is small compared to for instance the thermal expansion, a conclusion which prevails for most of the tests. Curve 2 in fig 26 illustrates the significantly different behaviour when the same load is applied before the temperature-rise. The temperature programs in both cases are virtually the same. When the temperature rise takes place under sustained load the thermal expansion is prevented to a degree that only partly can be attributed to the change in stress-strain relation and the development of creep.

It is clear that creep in a conventional sense plays a very limited role in an overall constitutive law. Only at temperatures above 400°C it may have some significance. This is indicated in figs 27a and b, where the creep vs. time during 3 hrs is shown for two stress levels and several different temperature levels.

An examination of the test data in series C shows that the creep may to a good approximation be related to the ratio v_T between the actual stress σ and the strength $\sigma_u(T)$ at each test temperature. Supposing that the creep is proportional to this ratio, at least in some interval, we can plot the 3 hour creep, $\epsilon_{c,3}$ divided by v_T , against temperature, fig 28. If linearity between ϵ_c and v_T is prevalent this plot will fall into one single curve. This is not exactly true, there is a rather large scatter for temperatures above 400°C , but there is little evidence that this depends on non-linearity between $\epsilon_{c,3}$

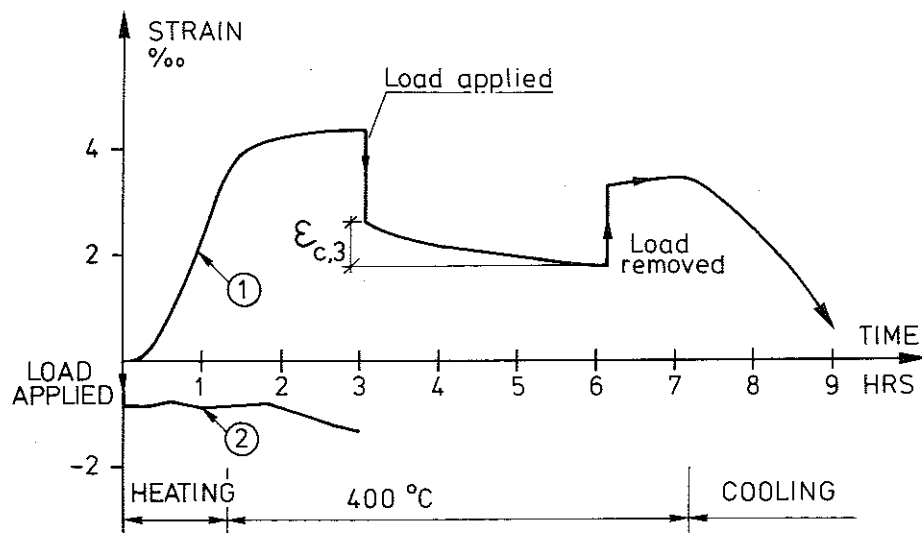


Fig 26 Measured total strain vs. time for typical test (C 27) in series C (curve 1), compared with the strain obtained if the load is applied from the beginning (curve 2, test D11). The temperature program is the same in both cases.

and v_T . It is therefore reasonable to write

$$\epsilon_{c,3} = v_T \cdot \phi_T(T) \quad (3.1a)$$

where $v_T = \frac{\sigma}{\sigma_u(T)}$

It can be found by inspection that the data fit well if

$$\phi_T(T) = \beta_o \cdot e^{k_1(T - 20)} \quad (3.1b)$$

where β_o and k_1 are constants.

By plotting $\log(\epsilon_{c,3}/v_T)$ against T we can determine the constants β_o and k_1 . Regression analysis of the data shown in fig 28 gives

$$\beta_o = 0.53 \cdot 10^{-3} \quad (3.1c)$$

$$k_1 = 3.04 \cdot 10^{-3} \text{ } ^\circ\text{C}^{-1}$$

The curve corresponding to the regression line is shown in fig 28.

Eq (3.1) gives an expression for the creep $\epsilon_{c,3}$ after 3 h as affected by stress and temperature when these two parameters are held constant. The influence of time may be expressed with a power function as follows

$$\epsilon_c = \epsilon_{c,3} \cdot \left(\frac{t}{t_r}\right)^p \quad (3.2)$$

where ϵ_c = creep after time t under constant stress and temperature
 $\epsilon_{c,3}$ = ditto after 3 h
 t = time
 t_r = reference time = 3 h
 p = dimensionless constant.

The time dependence is rather difficult to evaluate from the tests, but inspection of the data shows that a reasonable estimate of p is 0.5.

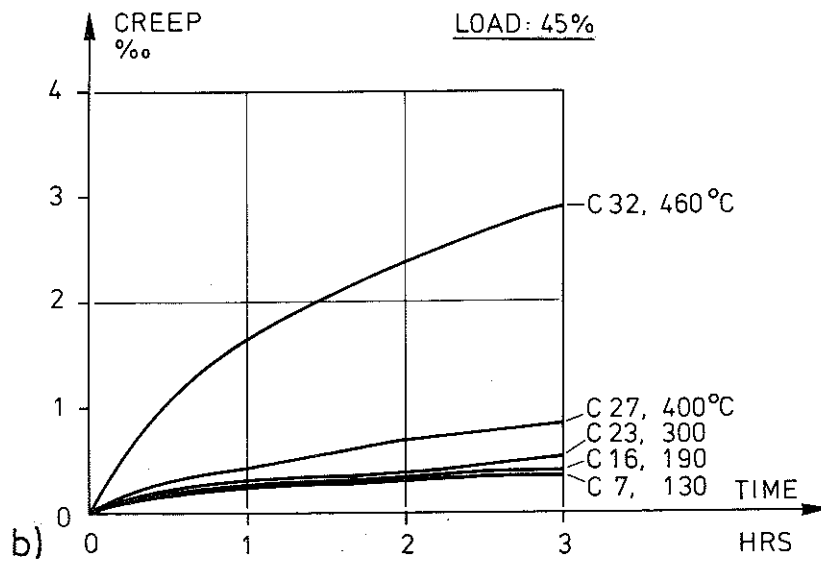
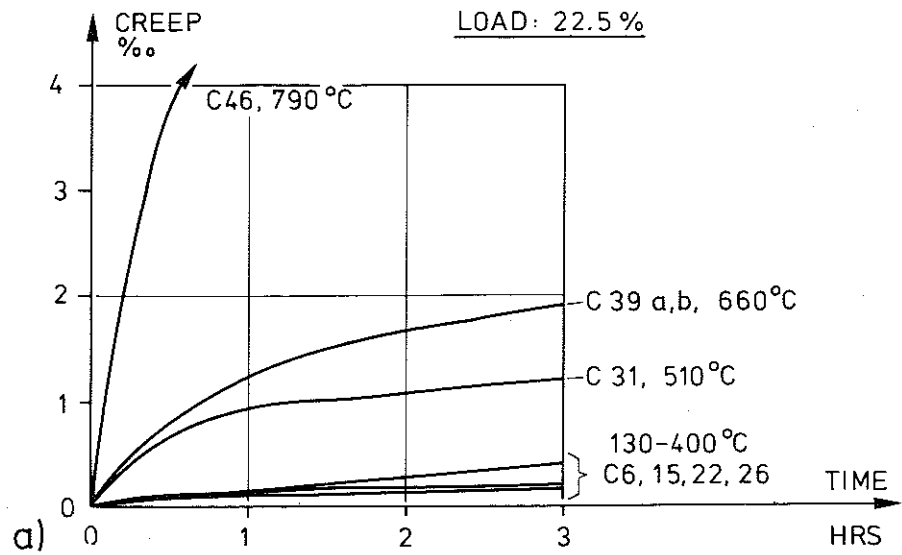


Fig 27 Creep vs. time at different temperature levels.
a) Stress level: 22.5 %
b) Stress level: 45 %

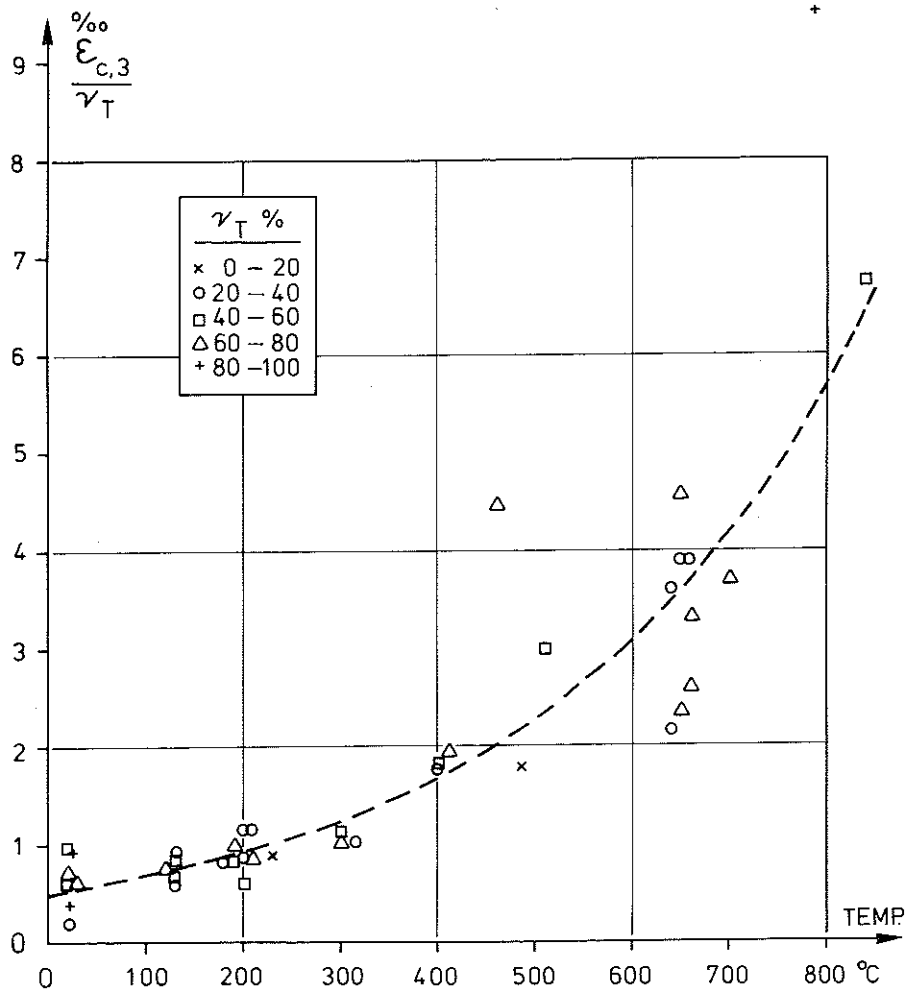


Fig 28 Plot of $\epsilon_{c,3}/\gamma_T$ vs. temperature T. The broken line represents the best fit of eq (3.1).
 $\epsilon_{c,3}$ = 3 hrs creep
 γ_T = ratio between stress σ and high temperature strength $\sigma_u(T)$.

In this section a constitutive model is derived , describing the mechanical behaviour known from tests as close as possible. The model presented herein is developed on a purely phenomenological basis directly connected to data obtained from different types of tests. The formulation is made with the purpose of using it in computer analysis of structural behaviour.

Generally, the constitutive law for concrete under high temperatures may be expressed as follows:

$$\epsilon = \epsilon (\sigma(t), T(t), \overset{\sim}{\sigma}) \quad (4.1)$$

where

ϵ = total strain at time t

σ = stress

T = temperature

$\overset{\sim}{\sigma}$ = stress history

An adequate formulation of the model is obtained if the total strain is seen as the sum of four different strain components each of which is connected to and correlated with a specified type of test. The strain components are

Thermal strain, including shrinkage, measured on unstressed specimens under variable temperature.

Instantaneous stress-related strain, based on stress-strain curves obtained under constant stabilized temperature.

Creep-strain, time dependent strain recorded under constant stress at constant stabilized temperature.

Transient strain, accounting for the effect of temperature increase under stress, derived from tests under constant stress and variable temperature.

Or, formulated mathematically:

$$\epsilon = \epsilon_{th}(T) + \epsilon_{\sigma}(\sigma, \sigma, T) + \epsilon_{cr}(\sigma, T, t) + \epsilon_{tr}(\sigma, T) \quad (4.2)$$

where

- ϵ = total strain
- ϵ_{th} = thermal strain
- ϵ_{σ} = stress-related strain
- ϵ_{cr} = creep strain
- ϵ_{tr} = transient strain

The usual sign convention is used here , positive sign for tensile stresses and strains and negative for the compressive ones. Parametric formulations for each of these strain components are described and evaluated on the basis of test results reported in the literature and in this paper. The validity of the model thus obtained is checked against test data covering varying combinations of stress and temperature histories. The treatment is limited to stress histories where $\sigma \leq 0$, i.e. compressive stresses. No test data are available for the behaviour under tensile stresses or in cases where the stresses change sign. When the model is applied in a structural analysis the behaviour under tension may be described by introducing relatively simple assumptions, see /14/. This is justified in many cases by the fact that the tensile stresses in the concrete are relatively insignificant as regards the structural behaviour.

4.1 Thermal strain

The thermal strain during heating is a simple function of the temperature directly given by the measured thermal expansion curve. Since drying shrinkage is included, the thermal expansion depends on the initial moisture content. The tests, cf. fig 18, also show that the thermal expansion depends on the rate of heating, but this is probably an effect of the variation in temperature distribution and is therefore neglected in the model.

4.2 Instantaneous, stress-related strain

The calculation of the stress-related strain is based on the concept that at every state a stress-strain relation is valid for the material. This stress-strain relation should be such that it appropriately reflects the response of the material to a change in stress. From the behaviour known from testing this means that the stress-strain relation at a given time should depend on the current temperature and the pre-history of stress, c.f. eq (4.2).

The general description of the stress-strain relation is shown in fig 29. The curve consists of a parabolic branch followed by a linear descending branch /15/. This description was chosen among a number of other suggestions found in the literature, due to its relative simplicity and due to the fact that a computer subroutine for its present application was available in /15/.

The boundary conditions of the parabolic curve in fig 29 are

$$\sigma = 0 \text{ when } \epsilon_{\sigma} = 0 \quad (4.3 \text{ a})$$

$$\sigma = \sigma_u \text{ when } \epsilon_{\sigma} = \epsilon_u \quad (4.3 \text{ b})$$

$$\frac{\partial \sigma}{\partial \epsilon_{\sigma}} = 0 \text{ when } \epsilon_{\sigma} = \epsilon_u \quad (4.3 \text{ c})$$

where

σ_u = ultimate stress at the current temperature

ϵ_u = strain at ultimate stress, ultimate strain.

These boundary conditions yield the following equation for the parabolic branch

$$\sigma = \sigma_u \cdot \frac{\epsilon_{\sigma}}{\epsilon_u} \left(2 - \frac{\epsilon_{\sigma}}{\epsilon_u} \right) \quad 0 \leq \epsilon_{\sigma} \leq \epsilon_1 \quad (4.4)$$

where $\epsilon_1 < \epsilon_u$ is the strain at transition between the parabolic branch and the linear descending branch. The initial fictitious elastic

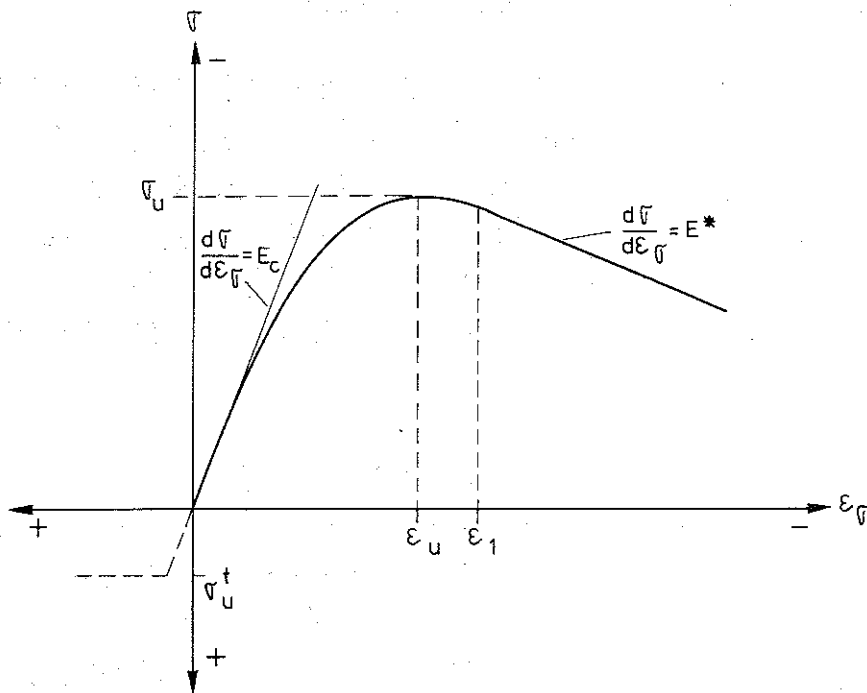


Fig 29 General description of the stress-strain relation used in the material model.

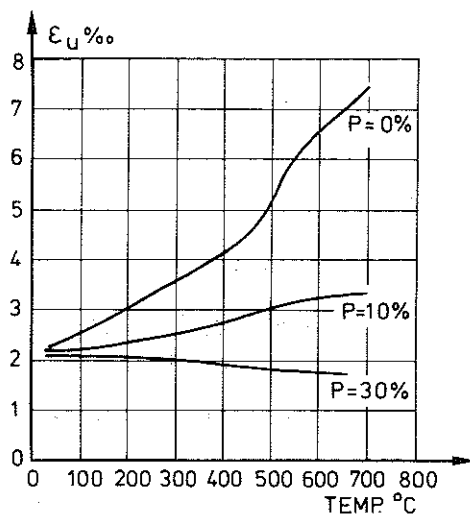


Fig 30 Ultimate strain ϵ_u as a function of temperature for specimens stressed at different levels, P , during the heating period /9/.

modulus E_c (when $\varepsilon \rightarrow 0$) is then obtained from eq (4.4):

$$E_c = 2 \cdot \frac{\sigma_u}{\varepsilon_u} \quad (4.5)$$

The linear descending portion of the stress-strain envelope in compression is given by

$$\sigma = E^* \cdot \varepsilon_\sigma + \sigma^* \quad \varepsilon_1 > \varepsilon_\sigma \quad (4.6)$$

where

$$\sigma^* = \sigma_u \left(1 - \frac{E^*}{E_c}\right)^2 \quad (4.7)$$

The transition point ε_1 between the two portions is obtained by

$$\varepsilon_1 = \left(1 - \frac{E^*}{E_c}\right) \varepsilon_u \quad (4.8)$$

Thus the stress-strain relation is uniquely defined if the three parameters σ_u , ε_u and E^* are known. The problem now is to express these parameters as functions of temperature and stress history. The description of the material model in this general context is made for the case when the stresses are negative during the whole history. For stress distribution calculations in section 5 the behaviour in tension is described by introducing the simple assumptions shown in fig 22.

4.2.1 Ultimate stress σ_u

The compressive strength of concrete at high temperature in percent of that at ambient conditions depends on a number of mixture parameters such as petrographical composition, cement-aggregate ratio and water-cement ratio, see e.g. /3/. The ultimate stress σ_u is clearly a function of temperature as shown in fig 22, for specimens loaded to failure at constant temperature conditions.

The fact that specimens heated under sustained low stress retain a somewhat higher strength than those unstressed during heating has been confirmed by several authors. However, the most realistic values of σ_u is probably obtained from tests where specimens under constant stress are heated to failure, see 2.2, fig 23. The scarce data available from these types of tests indicate that the relative strength may be somewhat higher than those obtained in normal testing, but the difference seems to be comparatively small.

In view of the uncertainties inherent in any estimation of high-temperature strength of concrete it is reasonable to estimate that σ_u is a unique function of temperature and that the influence of different prehistories of stress may be neglected. The relationship between σ_u and T can be obtained from the ordinary types of tests at constant temperatures shown in fig 22, which will be used in the present study unless otherwise stated.

4.2.2 Ultimate strain ϵ_u

The ultimate strain from stress-strain tests at constant temperature (test type B) is shown in fig 25 c. ϵ_u is significantly affected by the prehistory of stress. In fig 30 from /11/ the same effect is shown. The absolute value of ϵ_u increases monotonously with temperature for specimens being unstressed during heating, while if the specimens are stressed under heating with 30 % of the strength at ambient conditions, ϵ_u is almost unaffected by the temperature rise. Accordingly, in predicting ϵ_u at a given state, the influence of the previous stress history must be taken into account in some way or another.

It is logical to express the prehistory of stress at a given time by the accumulated transient strain ϵ_{tr} , see section 4.4 below, and write

$$\epsilon_u = \epsilon_u(T, \epsilon_{tr}) \quad (4.9)$$

In particular when $\epsilon_{tr} = 0$, i.e. when the previous stress history is equal to zero, the ultimate strain is given by the results in fig 24 or fig 30 ($P = 0$ %). Or

$$\epsilon_u(T, 0) = \bar{\epsilon}_u(T) \quad (4.10)$$

Noting that compressive strains are negative we can write

$$\epsilon_u(T, \epsilon_{tr}) = \min(\epsilon_{u0}, \bar{\epsilon}_u - \epsilon_{tr}) \quad (4.11)$$

where ϵ_{u0} = ultimate strain at ambient conditions and $\bar{\epsilon}_u = \bar{\epsilon}_u(T)$ = ultimate strain at zero load history.

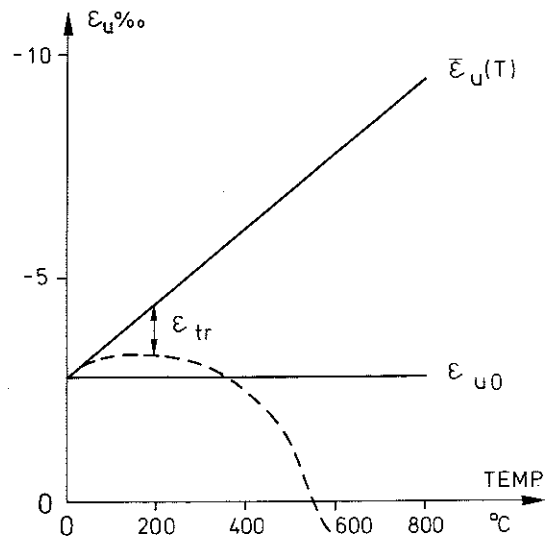


Fig 31 Illustration of the calculation of ϵ_u in the material model.

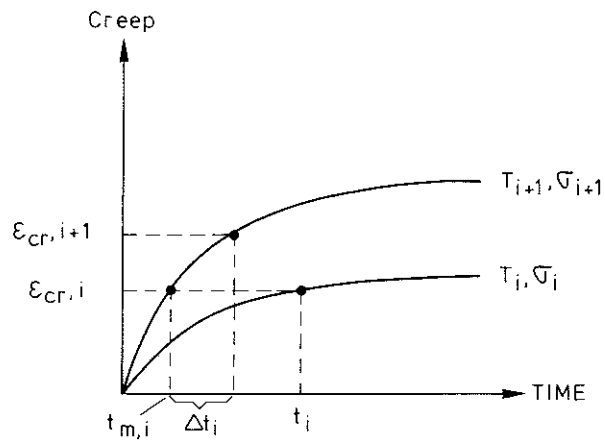


Fig 32 The principle of strain hardening for creep.

This means that the absolute value of the ultimate strain is reduced by an amount equal to $|\epsilon_{tr}|$, due to a prehistory of stress, but is always greater than or equal to the ultimate strain at ambient conditions. This is illustrated in fig 31 where a typical variation of ϵ_u is shown. Below $\approx 350^\circ \text{C}$ ϵ_u is equal to $\bar{\epsilon}_u - \epsilon_{tr}$ while above this temperature ϵ_u is equal to ϵ_{u0} . For simplicity $\bar{\epsilon}_u$ is expressed by a linear relation with temperature.

4.2.3 Slopes of descending branch, E^*

There is very little information in literature as concerns the descending branch of the stress-strain curve. The choice of this parameter is however not very important for the behaviour and E^* is given the constant value - 880 MPa independent of temperature and stress history as assumed in /14, 15/.

It should be pointed out that the behaviour of the concrete is difficult to predict in this region. In an actual structure the shape in the descending region depends in a decisive way on the stress gradient, the arrangement of reinforcement and so forth /16/. It is questionable if the behaviour found in stress-strain tests on nonreinforced specimens is representative for the behaviour in actual structures.

It might be suggested that a limiting strain when crushing of the concrete takes place should be defined /15/. But such a limit is also difficult to specify generally, it depends in a decisive way on the actual application. In fact a material model of the type described herein is not very well suited to predict the behaviour in the failure state and it is necessary to consider separate criteria for failure depending on the structural problem in question. These problems are beyond the scope of the present paper.

4.2.4 Variable stress and temperature

The basic input into a calculation of the stress-related strain is the stress-strain relation, which is uniquely defined at a given state. For an arbitrary temperature and stress history the calculation of ϵ_σ is made in a time step iteration. The incremental change between two time steps is either a loading or an unloading process, depending on the change in stress and temperature. It is assumed that the stress σ_{i-1} , the stress-related strain $\epsilon_{\sigma,i-1}$ and the temperature T_{i-1} are known at a time t_{i-1} . For the subsequent time $t_i = t_{i-1} + \Delta t_{i-1}$ the temperature T_i is always known. To determine whether unloading or loading is prevalent for the time step the permanent inelastic strain $\epsilon_{0,i-1}$ at the previous time t_{i-1} is used. This is given by

$$\epsilon_{0,i-1} = \min \left(\epsilon_{0,i-2}, \epsilon_{\sigma,i-1} - \frac{\sigma_{i-1}}{E_{c,i-1}} \right) \quad (4.12)$$

Depending on the application two different situations may be valid, one is that the stress σ_i at time t_i is known and $\epsilon_{\sigma,i}$ is unknown and the other is that $\epsilon_{\sigma,i}$ is known and σ_i should be determined.

If the stress σ_i is known the stress-strain envelope valid at time t_i is determined from the temperature T_i and the stress history up to t_i . In this way ϵ_σ is expressed as a function of σ according to

$$\epsilon_\sigma = f_i(\sigma) \quad (4.13)$$

where f_i denotes the stress-strain relation valid at the current time t_i . $\epsilon_{\sigma,i}$ is then given by

$$\epsilon_{\sigma,i} = \min \left(f_i(\sigma_i), \epsilon_{0,i-1} + \frac{\sigma_i}{E_{c,i}} \right) \quad (4.14)$$

If instead the strain $\epsilon_{\sigma,i}$ is given from the outset the stress is obtained by

$$\sigma_i = \max \left(f_i^{-1}(\epsilon_{\sigma,i}), E_{c,i}(\epsilon_{\sigma,i} - \epsilon_{0,i-1}) \right) \quad (4.15)$$

where f_i^{-1} is the inverse of the relationship f_i defined above.
Note that compressive stresses and strains are defined as negative in the above relations.

4.3 Creep strain, ϵ_{cr}

According to eqs (3.1) and (3.2) the basic creep ϵ_{cr} at constant temperature and constant stress is expressed by

$$\epsilon_{cr} = \beta_o \cdot \frac{\sigma}{\sigma_u(T)} \left(\frac{t}{t_r}\right)^p \cdot e^{k_1 \cdot (T-20)} \quad (4.16)$$

where

$$\beta_o = -0.53 \cdot 10^{-3}$$

σ = stress

$\sigma_u(T)$ = ultimate stress at current temperature

t = time

$$t_r = 3 \text{ hrs}$$

$$p = 0.5$$

$$k_1 = 3.04 \cdot 10^{-3} \text{ } ^\circ\text{C}^{-1}$$

T = temperature

Eq (4.16) thus expresses the creep vs. time for any given combination of temperature and stress. When the temperature and the stress is varying with time the evaluation of ϵ_{cr} is based on the strain hardening principle in accordance with fig 32, which is formulated in the following procedure in a time step calculation, cf. /4/.

Assuming that the stress σ_i , the temperature T_i and the accumulated creep strain $\epsilon_{cr,i}$ is known at the time t_i , we want to obtain the accumulated creep strain $\epsilon_{cr,i+1}$ at a subsequent time $t_{i+1} = t_i + \Delta t_i$. If we know the temperature T_{i+1} and the stress σ_{i+1} at t_{i+1} we can calculate the material time $t_{m,i}$ that would give a creep equal to the accumulated value $\epsilon_{cr,i}$ at constant stress σ_{i+1} and constant temperature T_{i+1} . $t_{m,i}$ can be solved explicitly from eq (4.16)

$$t_{m,i} = t_r \left[\frac{\epsilon_{cr,i}}{\beta_0 \frac{\sigma_{i+1}}{\sigma_u(T_{i+1})} \cdot \exp \left\{ k_1 (T_{i+1} - 20) \right\}} \right]^{1/p} \quad (4.17)$$

By adding the actual time increment Δt_i to the material time $t_{m,i}$ we obtain

$$\epsilon_{cr,i+1} = \beta_0 \cdot \frac{\sigma_{i+1}}{\sigma_u(T_{i+1})} \cdot \left(\frac{t_{m,i} + \Delta t_i}{t_r} \right)^p \cdot \exp \left[k_1 (T_{i+1} - 20) \right] \quad (4.18)$$

If the stress σ_{i+1} is unknown when the creep strain is evaluated, the calculation may with sufficient accuracy be based on the stress σ_i at the previous time t_i .

4.4 Transient strain ϵ_{tr}

The transient strain ϵ_{tr} develops under stress when the temperature increases. Tests show that this strain is essentially irrecoverable and occurs only under the first heating of the concrete. This strain accounts for the temperature change effect, which will produce an instability of the material and activate the reactions responsible for the decomposition, cf /4/. It may be defined as that part of the total strain obtained in stressed concrete under heating that cannot be accounted for otherwise.

It is impossible to design tests where the transient strain component can be directly measured. But ϵ_{tr} may be evaluated from the tests of type A, where specimens under constant stress were heated to failure. ϵ_{tr} is obtained as the difference between the measured total strain ϵ_{tot} and the other three components, thermal, stress-related and creep strain, respectively, i.e.

$$\epsilon_{tr} = \epsilon_{tot} - \epsilon_{th} - \epsilon_{\sigma} - \epsilon_{cr} \quad (4.19)$$

When analysing the results of fig 17 ϵ_{th} was taken directly from the measured thermal expansion. The stress-related strain ϵ_{σ} and the creep strain were calculated according to the principles described in 4.2 and 4.3, respectively. As a result ϵ_{tr} is obtained as

a function of temperature. In analysing the tests in fig 17 it was found that ϵ_{tr} is reasonably linear with the stress σ . When plotting $\epsilon_{tr} / (\sigma/\sigma_{uo})$, where σ/σ_{uo} is the stress/strength ratio, against temperature, we obtain the relationship shown in fig 33. The figure shows clearly that the assumption of a linear relation between ϵ_{tr} and stress is justified. Thus we can write

$$\epsilon_{tr} = \frac{\sigma}{\sigma_{uo}} \cdot g(T) \quad (4.20)$$

where $g(T)$ is a function of temperature. Inspection of the data in fig 33 shows that $g(T)$ is approximately proportional to ϵ_{th} , i.e. the temperature dependence of the transient strain is very similar to that of the thermal strain. Accordingly

$$\epsilon_{tr} = -k_2 \frac{\sigma}{\sigma_{uo}} \cdot \epsilon_{th} \quad (4.21)$$

where k_2 is a dimensionless constant. When plotting $\epsilon_{tr}/(\sigma/\sigma_{uo})$ against ϵ_{th} for the data reproduced in fig 33 we obtain a reasonably straight line, see fig 34. Regression analysis of the data gives $k_2 = 2.35$ for these tests. The correlation is not so good for temperatures around and above 550°C and the data in this region are omitted. The behaviour at these high temperature is difficult to interpret due to the scatter in strength between the individual tests. Still the accuracy of the description is very good and sufficient for practical purposes.

To show this the complete model including a formulation of ϵ_{tr} according to eq (4.21) was applied on the tests shown in figs 17, 33 and 34. The result of this exercise is shown in fig 35, where measured and calculated strains in the tests A6a - A9 are reproduced.

The analysis described above was also performed for similar data reported in the literature. Weigler and Fischer /9/ tested specimens under sustained load being heated to 600°C and subsequently cooled. The measured strains during heating were correlated with eq (4.21), giving a value of $k_2 = 2.0$. The accuracy of this correlation is illustrated in fig 44 (the heating branch), showing measured and calculated results. Again the model gives a very good description of the behaviour.

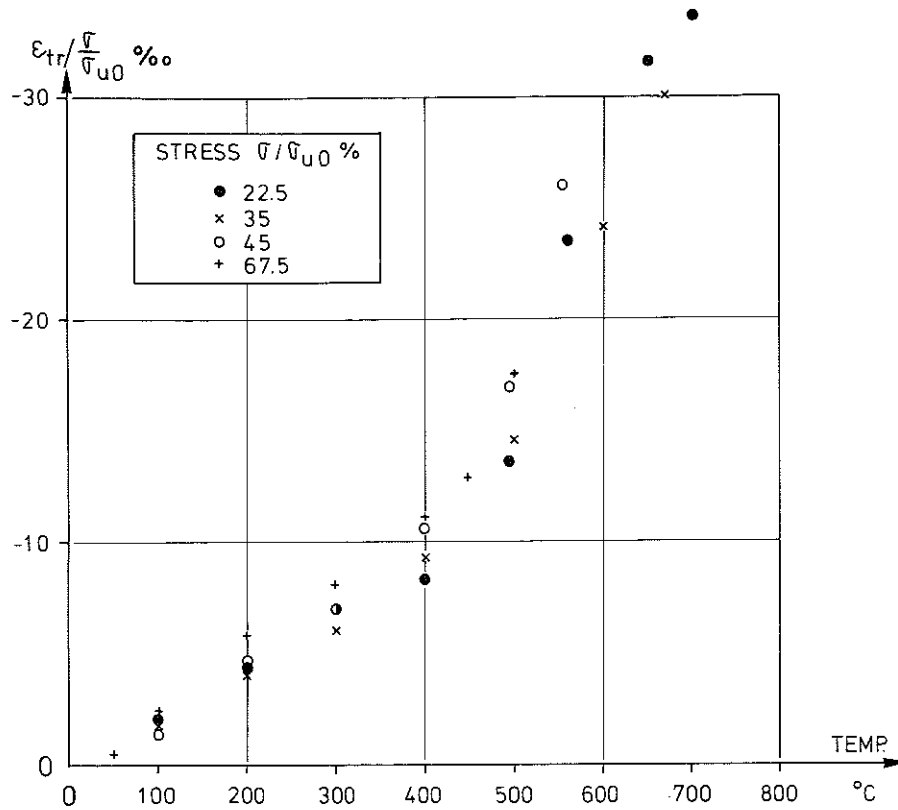


Fig 33 The ratio $\epsilon_{tr} / (\sigma / \sigma_{u0})$ as a function of temperature evaluated from the tests shown in fig 17.

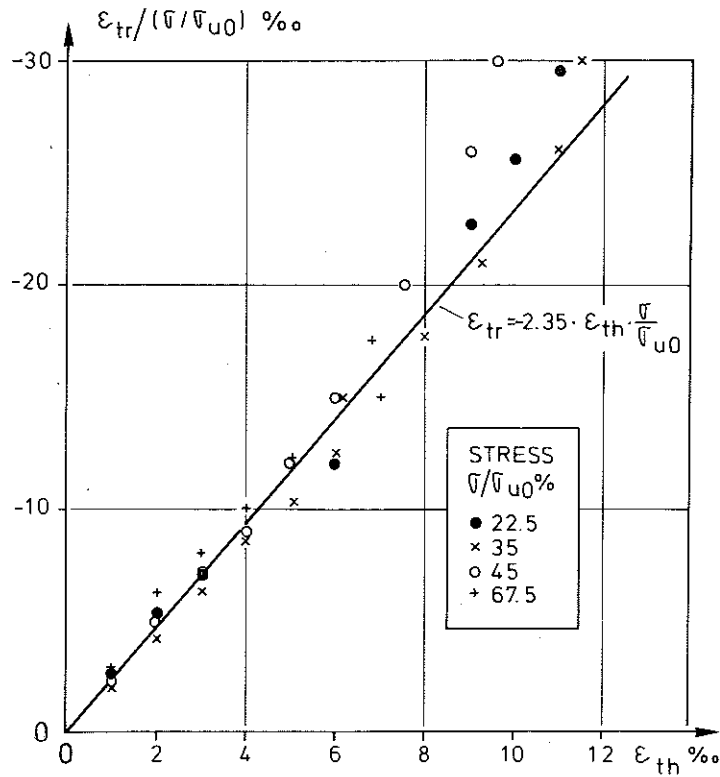


Fig 34 $\epsilon_{tr} / (\sigma / \sigma_{u0})$ plotted against the thermal strain ϵ_{th} for the tests shown in fig 17. The straight line is obtained from linear regression.

Schneider /10/ performed tests of the same type as those described in this report (type A). The correlation of his data with eq (4.21) is less significant, but the relation between $\epsilon_{tr}/(\sigma/\sigma_{uo})$ and ϵ_{th} is linear up to about 500° C. In this linear region k_2 is determined to 1.8.

Fig 36 illustrates the adequacy of the model in describing Schneider's tests. The figure shows a certain discrepancy between measured and modelled strains for temperatures above 500° C, but the agreement is generally acceptable.

As stated before the transient strain component is a very important component in the model. Fig 37 gives an impression of the relative order of magnitude for the different components and the predominance of the transient component is obvious.

4.5 Material behaviour under cooling

The discussion up till now has been limited to the case when the concrete is heated for the first time. In fire exposure situations we are often interested in analysing also the behaviour during the subsequent cooling period. The knowledge of the behaviour under cooling is somewhat limited, but a relatively accurate description may still be made. A reasonable assumption is that the prevalent stress-strain relation during cooling is defined by the state corresponding to the previous maximum temperature and it also seems that the transient strain increment should be equal to zero as soon as a decrease in temperature takes place. The creep strain may in view of its unimportance be evaluated in the same way under cooling as under heating even if there is no evidence confirming this behaviour. The only significant problem arises with the thermal strain as regards its degree of reversibility.

It is clear that the main part of the thermal expansion is reversible, but the irreversible component is not significant for quartz aggregate concrete heated above the quartz inversion limit /9/. However, as a

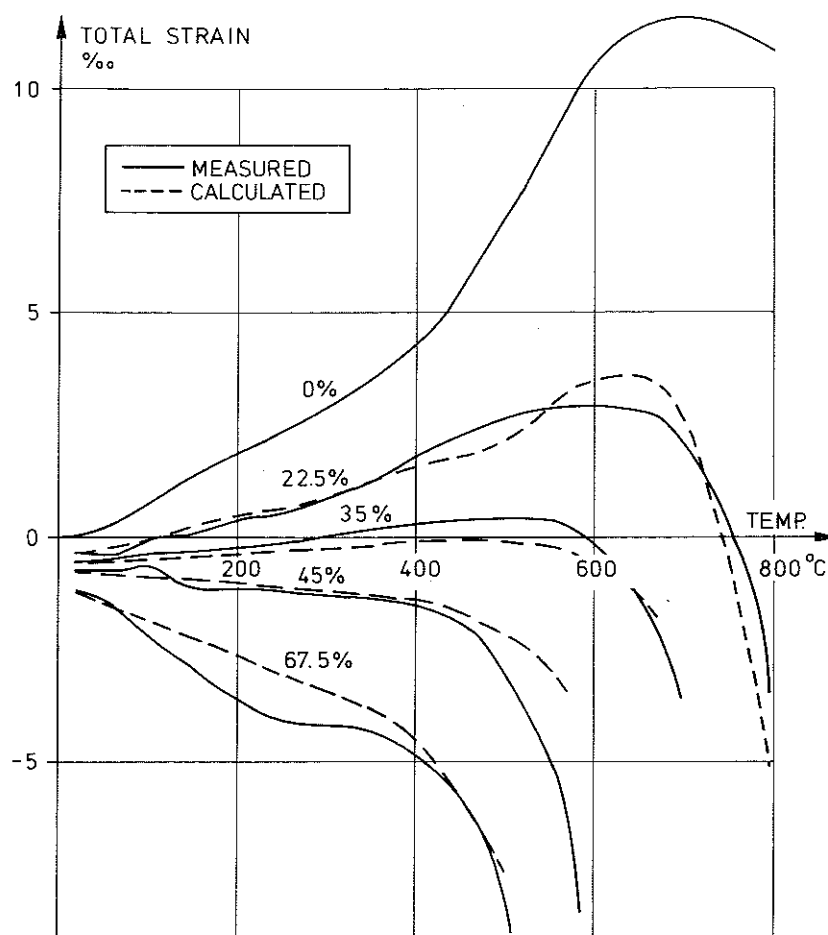


Fig 35 Deformation, including instantaneous strain at initial loading, upon heating ($5^{\circ} \text{C} \cdot \text{min}^{-1}$) for different levels of compressive stress (per cent of strength at ambient conditions). Full lines indicate experiments and the dashed lines are the results obtained from the material behaviour model ($k_2 = 2.35$).

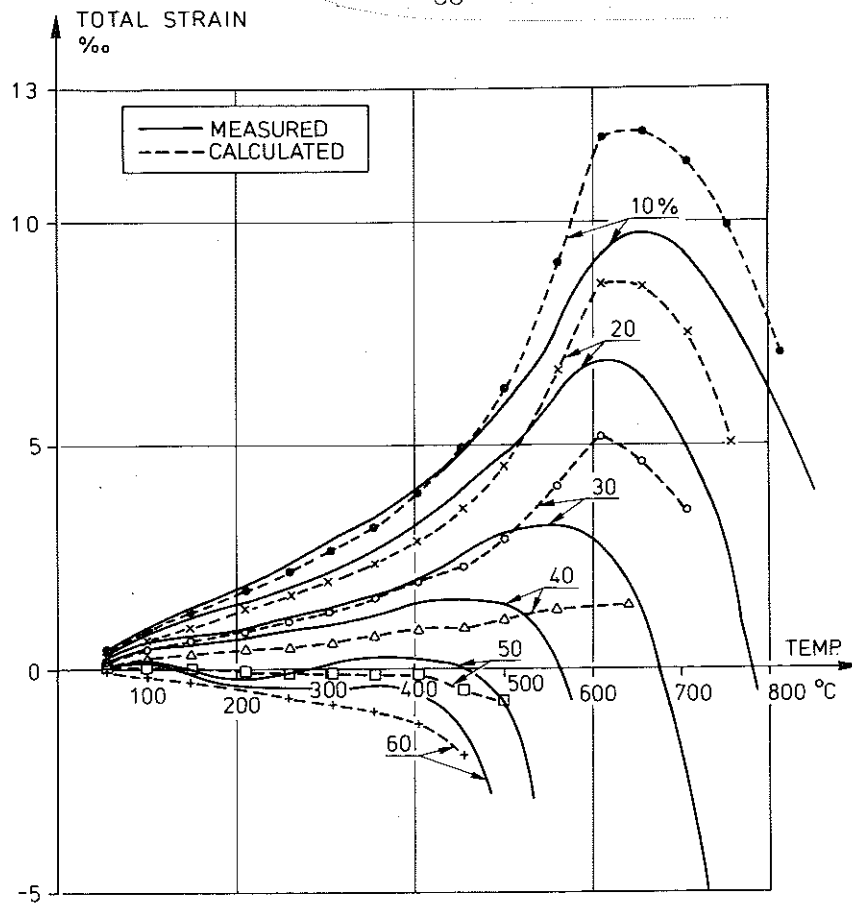


Fig 36 Deformation after initial loading upon heating ($2^{\circ} \text{C} \cdot \text{min}^{-1}$) for different levels of compressive stress. Full lines indicate experiments, /8/, and the dashed lines are the results obtained from the material behaviour model ($k_2 = 1.8$).

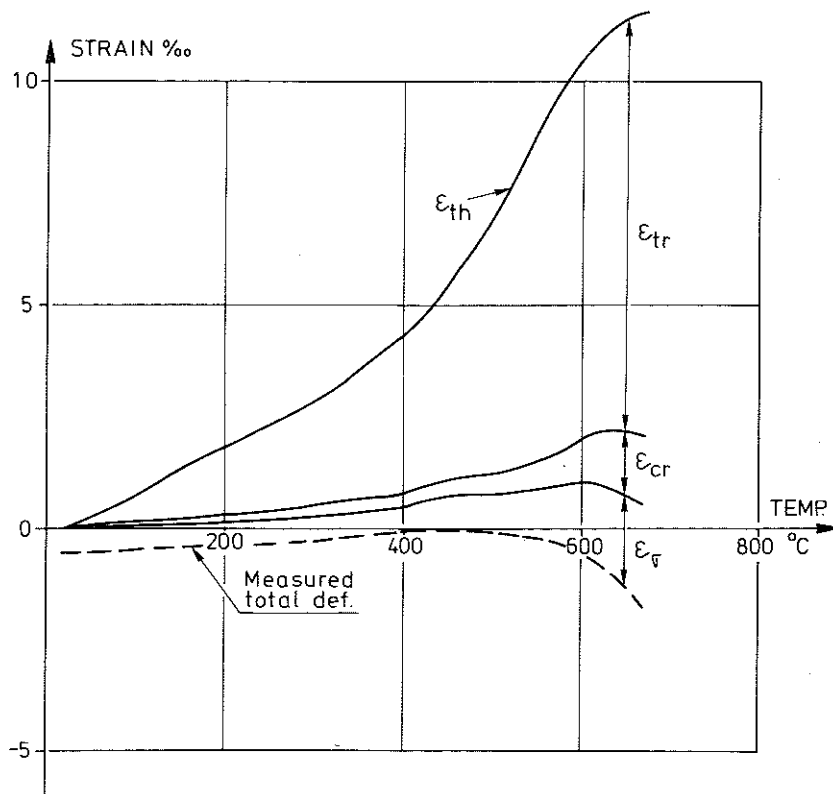


Fig 37 Relation between different strain components when the model is applied for test A 7 ($\sigma/\sigma_{u0} = 35\%$).

first approximation, pending more complete experimental information, it may be justified to assume that the thermal expansion is fully reversible.

4.6 Validity of the model

The material model described above has been quantitatively developed from four different types of tests each giving information of a specific strain component. The general validity of the model can be checked independently against other types of experiments with arbitrary load and temperature histories.

In the tests D1 - D4 of this report unloaded specimens were heated under restrained deformation and the restraint load was measured. The results from tests D2 and D4 are shown in fig 38. The rate of heating has no significant influence on the results. In fig 38 are also shown the corresponding results obtained from the material model ($k_2 = 2.35$) applied for these tests, the agreement being reasonably good.

The model was also compared with similar tests reported by Schneider /10, 11/, see fig 39. The figure shows the experimental and modelled strain behaviour for specimens heated under restrained deformation and at different levels of initial loading. The restraint load above 150°C is rather independent of the initial load, a behaviour which is predicted by the model. The quantitative agreement can also be regarded as fully acceptable.

Figs 40 and 41 show the observed and modelled strain behaviour in tests D5 - D8. In these tests the load was changed stepwise during the heating ($5^{\circ}\text{C}\cdot\text{min}^{-1}$). Again the model proves very reliable in predicting the behaviour.

Another example is shown in fig 42, referring to test D12, where the temperature was stabilized at 670°C after heating at a rate of $5^{\circ}\text{C}\cdot\text{min}^{-1}$ indicating that the behaviour at stabilized temperature is predicted in an essentially correct way.

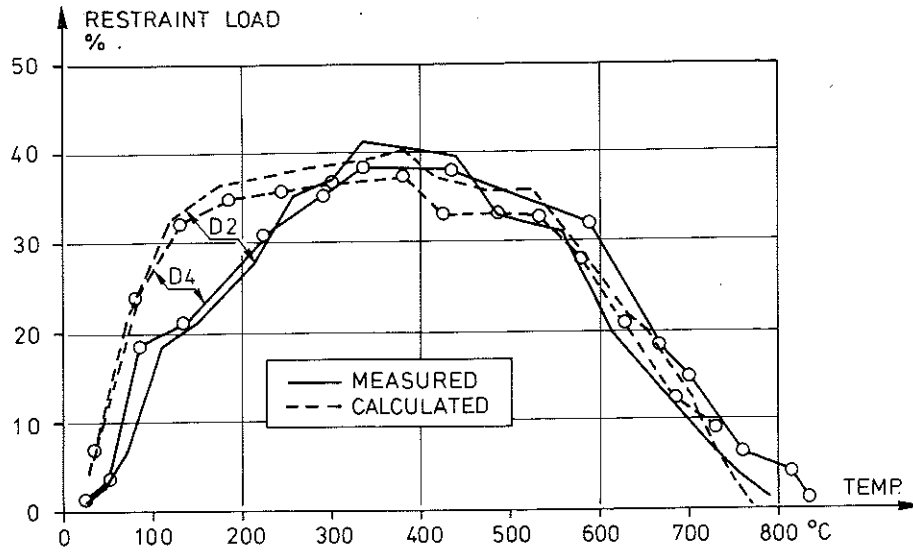


Fig 38 Measured and calculated restraint load (in per cent of ultimate load at ambient conditions) as a function of temperature for specimens being heated under fully restrained expansion. Rate of heating: $5^{\circ}\text{C} \cdot \text{min}^{-1}$ (D2) and $1^{\circ}\text{C} \cdot \text{min}^{-1}$ (D4)

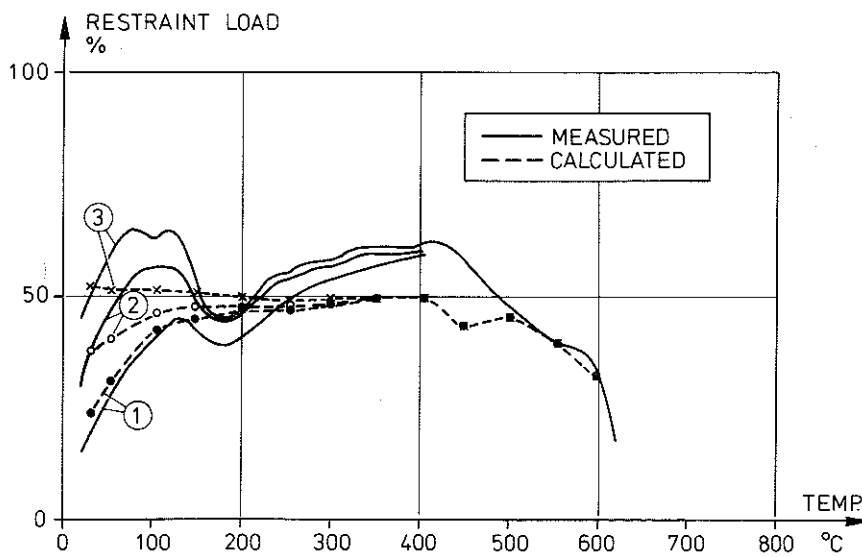


Fig 39 Measured /8/ (full lines) and calculated (dashed lines) restraint load (per cent of ambient strength) as a function of temperature for specimens heated under fully restrained expansion. Rate of heating: $2^{\circ}\text{C} \cdot \text{min}^{-1}$. Initial loading: 15 (1), 30 (2) and 45 % (3) of ultimate load at ambient conditions.

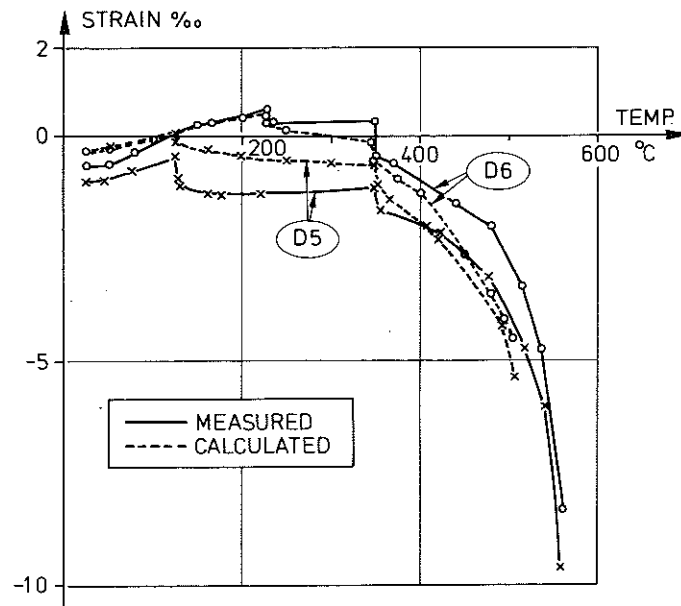


Fig 40 Measured and calculated strains in tests D 5 and D 6, cf. table 5.

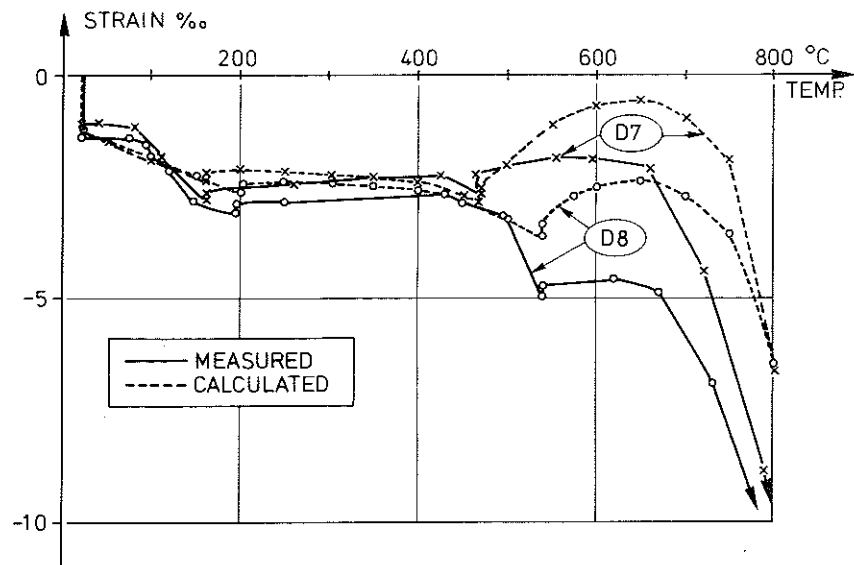


Fig 41 Measured and calculated strains in tests D 7 and D 8, cf. table 5.

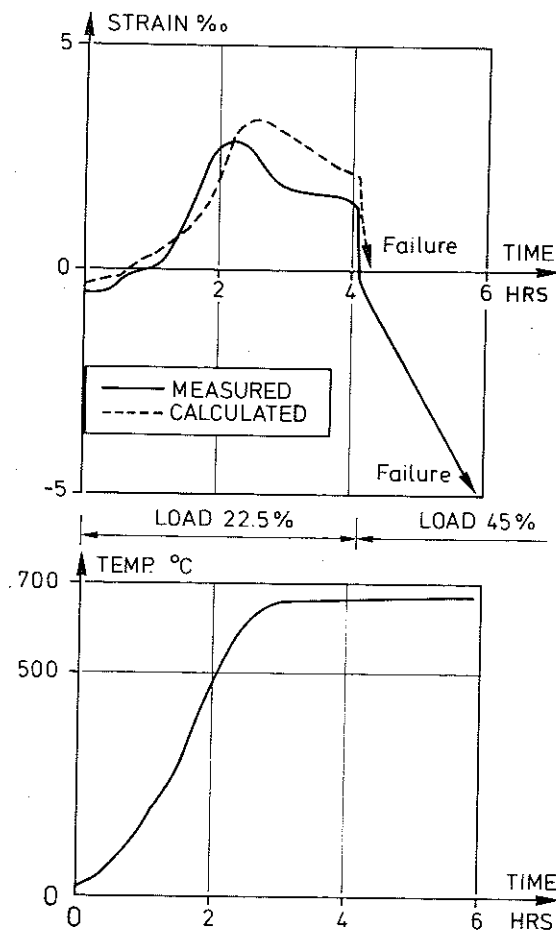


Fig 42 Measured and calculated strains in test D 12, cf. table 5. The temperature in the specimen vs. time is shown in the lower diagram.

The reliability of the model in cases where cooling takes place is illustrated in figs 43 and 44. Fig 43 shows a comparison between modelled and measured strains for test D 11, see table 5. A load equal to 45 % of the ambient strength was applied from the beginning and the specimen was subjected to a temperature treatment according to fig 43 b. After 3 hrs the load was increased to 67.5 %. The temperature drop between 5 and 7 hrs was due to a temporary loss of power to the furnace. The agreement between the model and the measured behaviour is remarkable in view of the complex temperature variation. Upon cooling there is a tendency to overestimate the contraction, as a result of the assumption that the thermal strain is fully reversible, cf. 4.5.

This tendency is even more marked when the maximum temperature exceeds the range 500 - 600° C, which is shown in fig 44, comparing the model with the results reported in /9/. Obviously, a more accurate prediction of the behaviour requires that the thermal strain is divided into reversible and irreversible components. To this end more experimental information is needed.

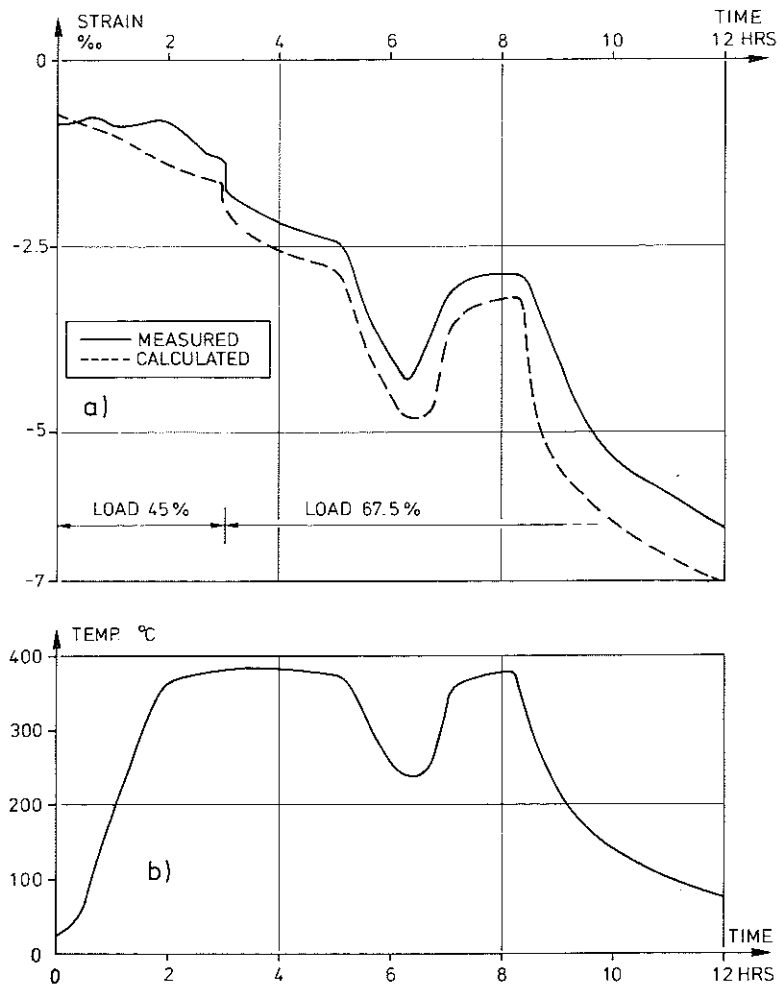


Fig 43 Measured and calculated strains in test D 11, cf. table 5. The temperature in the specimen is shown in the lower diagram.

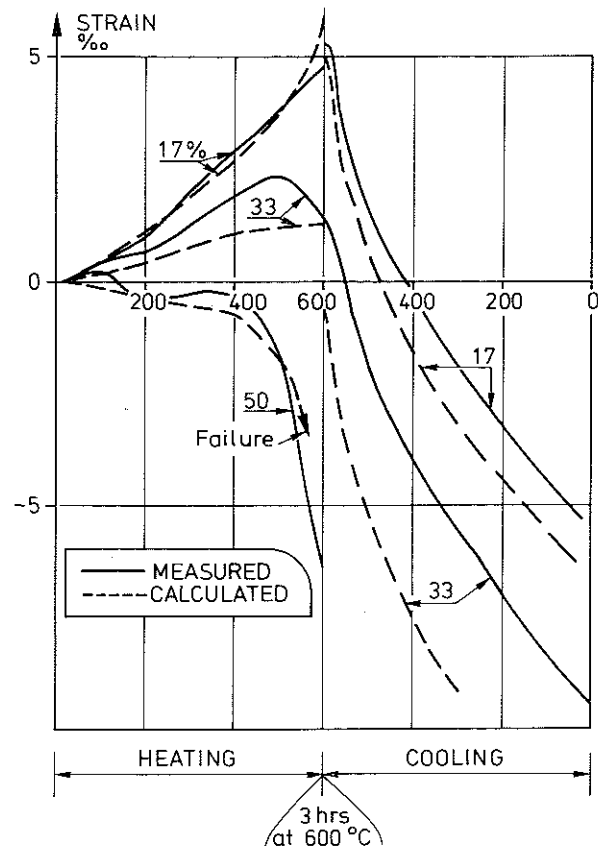


Fig 44 Deformation (after initial loading) upon heating to 600° C and subsequent cooling for different levels of compressive stress (per cent of strength at ambient temperature). Full lines indicate experiments /7/ and the dashed lines are the results obtained from the material behaviour model ($k_2 = 2.0$).

To illustrate the significance of the model in a simple way, it has been applied in calculating stress distributions and deformations for a circular cross section (diameter 150 mm) under sustained axial compressive load and exposed to axisymmetrical heating. The circular cross section was divided into 7 ringshaped elements, assuming constant stress within each element. Applying the material model for each element in a time step calculation together with the equilibrium and compatibility equations, the formal stress distribution and the overall strain for the cross section are obtained.

The calculation were made with different rates of external heating ($2, 4$ and $8^{\circ} \text{C} \cdot \text{min}^{-1}$) and with different levels of compressive load ($0, 20, 40$ and 60% of ultimate load at ambient conditions). For the case with zero load tensile stresses are obtained in some parts of the cross section and an assumption has to be made as regards the behaviour in tension. This assumption was made very simple, viz. that the increments of ϵ_{cr} and ϵ_{tr} is neglected in tension and ϵ_{σ} is determined by an elasto-plastic stress-strain diagram as shown in fig 29. The ultimate tensile stress or the "yield stress" was assumed to vary with the temperature according to fig 45 /17/. This simple description is probably adequate for the present problem if we remember the simplification when the results are interpreted.

The temperature distributions at selected times are shown in fig 46 for the three rates of heating and the corresponding stress distribution obtained at an axial level of 40% are shown in fig 47. As can be seen in fig 47 the redistribution of stresses is very small as long as the temperatures in the outer parts are lower than about 400°C , in spite of the large temperature gradients. After that the stresses decrease in the outer zone and increase markedly in the central core. This is simply due to the fact that the strength falls rapidly above 400°C . This behaviour is however not valid when the temperature gradients are small, see fig 47 a.

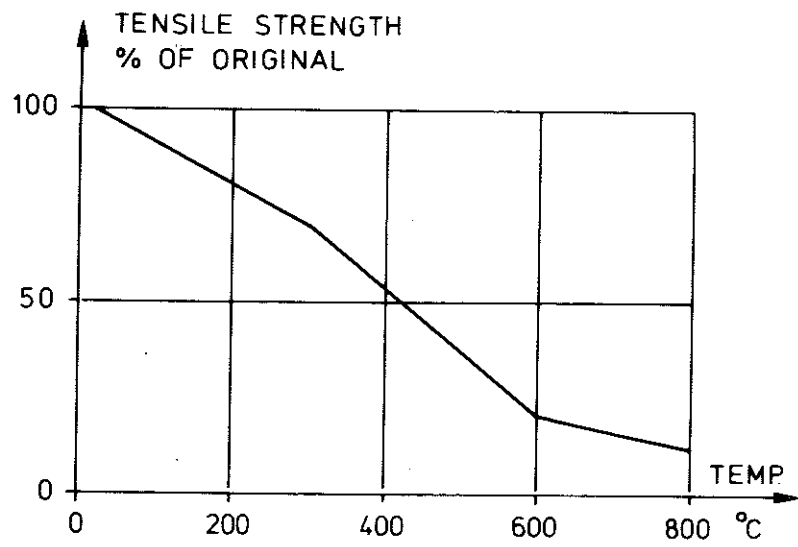


Fig 45 Tensile strength vs. temperature used in the example calculation in chapter 5.

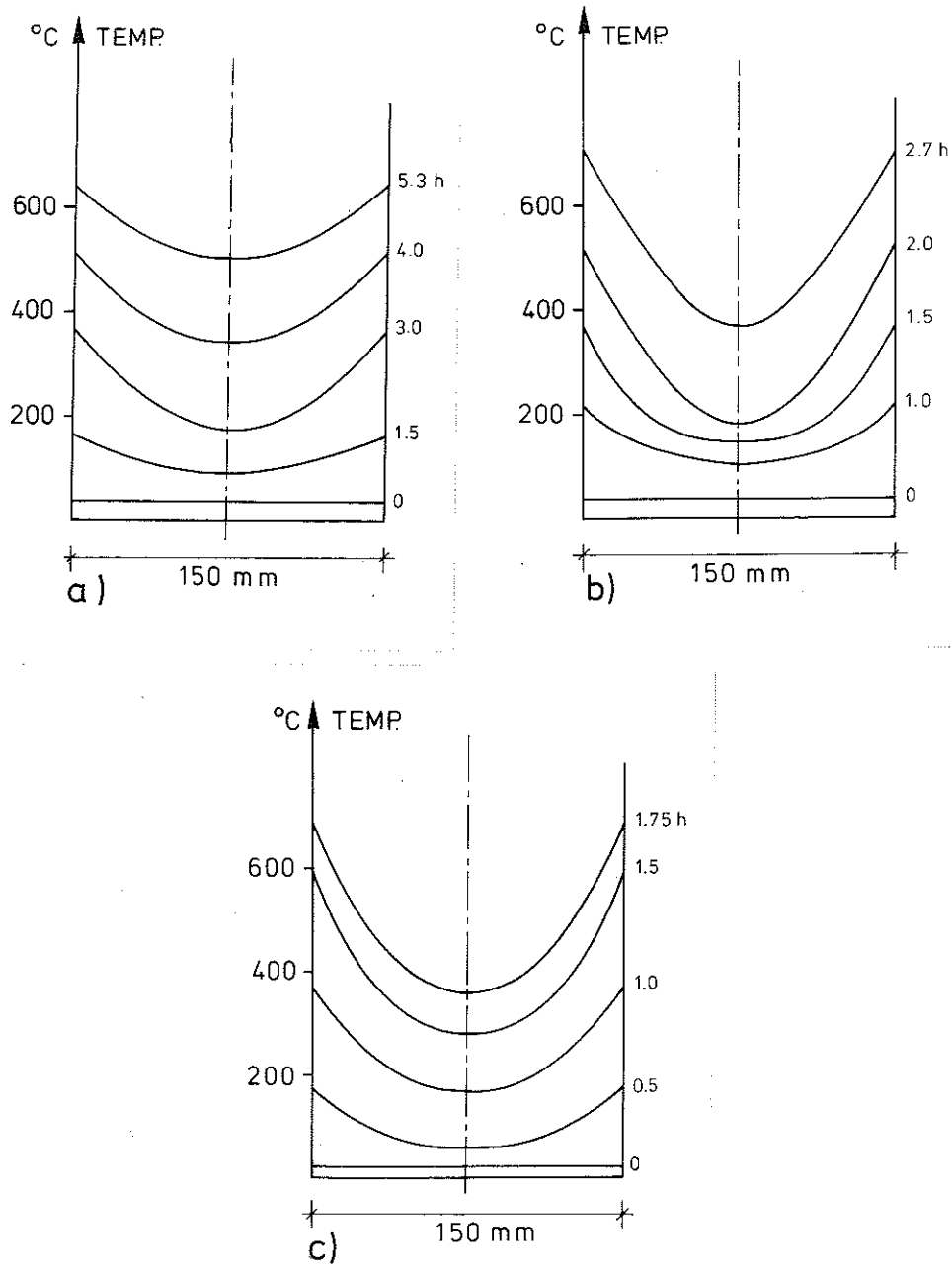


Fig 46 Transient temperature fields at selected times for circular cross section externally heated at constant rates.
a) $2^{\circ} \text{C} \cdot \text{min}^{-1}$
b) $4^{\circ} \text{C} \cdot \text{min}^{-1}$
c) $8^{\circ} \text{C} \cdot \text{min}^{-1}$

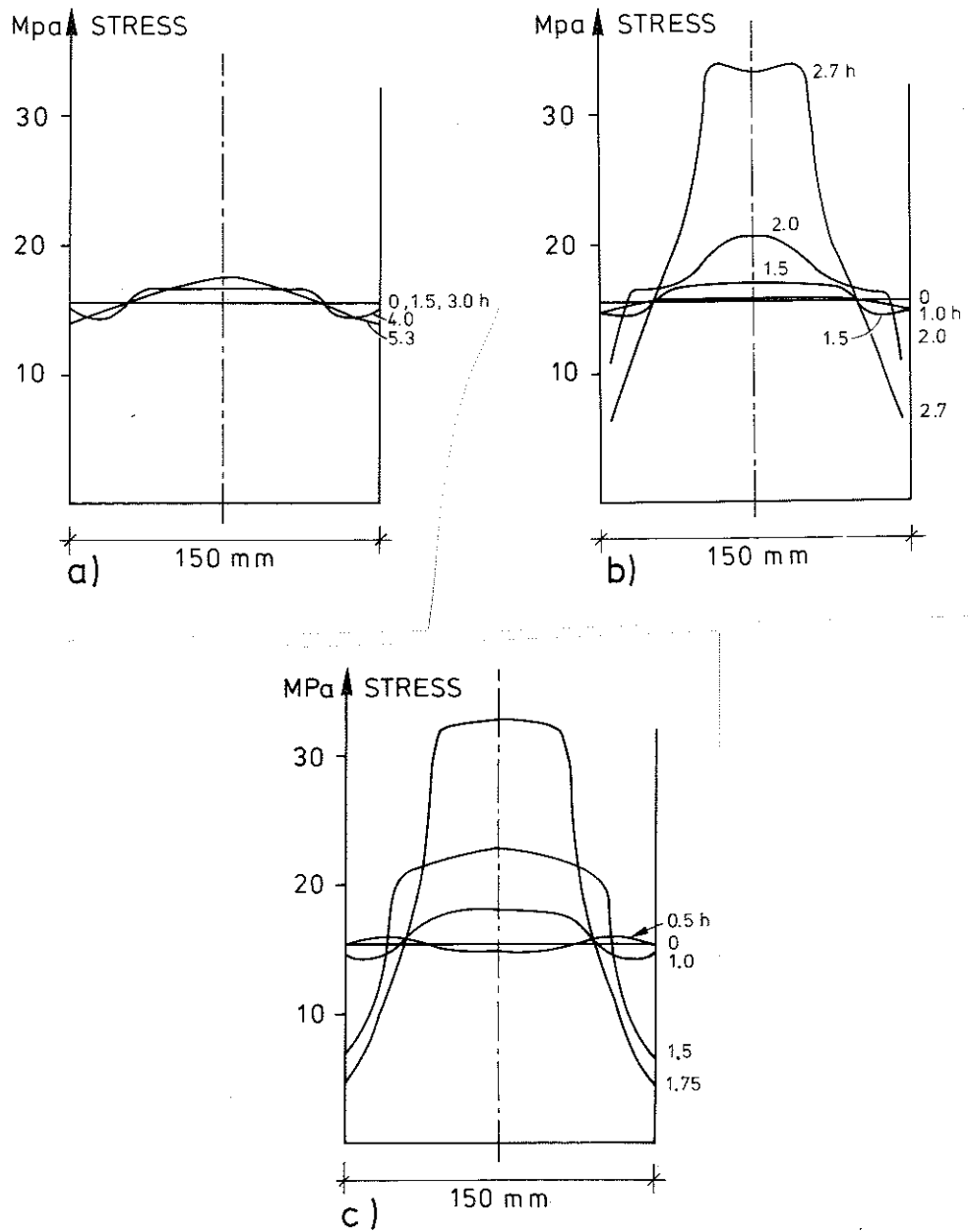


Fig 47 Calculated stress distributions for an axially loaded cylindrical column under transient thermal exposure, see fig 45. Load level: 40 % of ultimate load at ambient conditions. Rate of heating: a) $2^{\circ}\text{C} \cdot \text{min}^{-1}$
b) $4^{\circ}\text{C} \cdot \text{min}^{-1}$
c) $8^{\circ}\text{C} \cdot \text{min}^{-1}$

In fig 48 is shown the influence of load level on the stress distribution. The figure shows the stresses obtained for the most extreme thermal exposure, $8^{\circ} \text{C} \cdot \text{min}^{-1}$, for the load levels 0, 20 and 60 %. The corresponding results for 40 % is reproduced in fig 47 c.

At high load levels the stress tends to be concentrated in the central core after some time. The expected behaviour with thermal stress concentration in the outer, hot zone is only found to some extent when the static load is small and then mostly in the early stages of heating. As a rule, the formal stress distributions illustrated in figs 47 and 48 are very different from that obtained in an elastic stress analysis. In fact the response of the concrete is such that the so called thermal stresses will be very insignificant or even nonexistent. It can be concluded that stresses due to restrained thermal expansion cannot in themselves contribute to compression failure of the concrete and it is quite obvious that an elastic stress analysis bears little resemblance with reality.

It should be born in mind that the stresses calculated in this way are more or less formal values that are very sensitive to the detailed assumptions employed in the model. Still it is believed that the above analysis serves to illustrate the behaviour of concrete under thermal exposure in a very realistic way. The total deformation for the three cases in fig 47 are shown in fig 49 as a function of time. Comparing this diagram with fig 47 we can see that the large distributions of stress correspond to a rapid increase of the compressive strains. It can thus be concluded that very large temperature gradients have a certain influence on the total strain behaviour at the same load level.

In view of this fact the question arises whether the concept of a characteristic temperature used in the presentation and analysis of the results from tests under transient conditions, see 3.3 and 4.4, is adequate. To investigate the relevance of this concept under different rates of heating, a similar stress analysis was performed for the test specimens (75 mm diameter) exposed to the different rates of heating shown in fig 12 and loaded in the same way as in the tests. The thermal gradients shown in fig 12 are comparatively

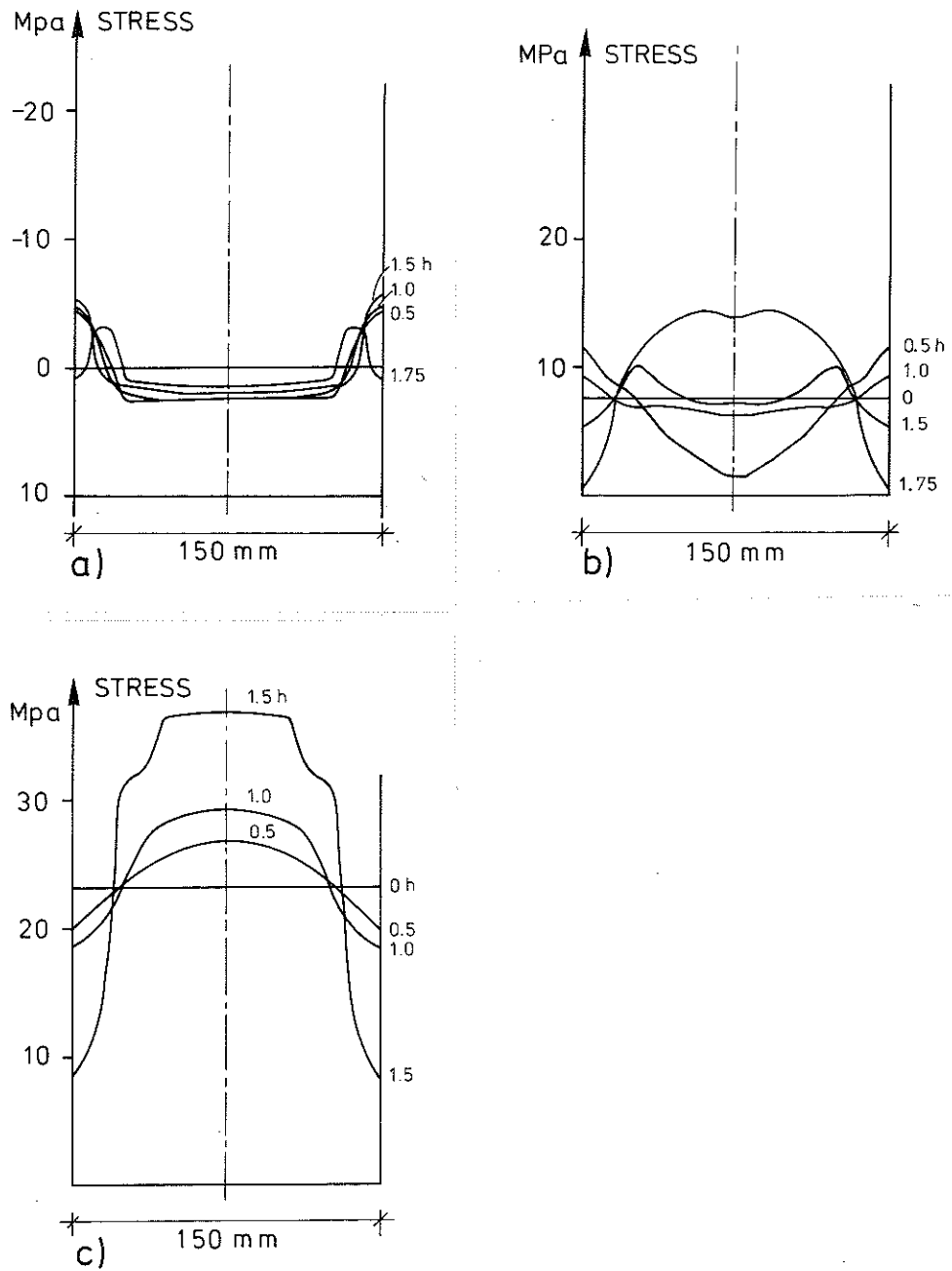


Fig 48 Calculated stress distributions for an axially loaded cylindrical column under transient thermal exposure. The rate of heating is $8^{\circ}\text{C} \cdot \text{min}^{-1}$, yielding the temperature distributions shown in fig 45 c. Load level: a) 0 % b) 20 % c) 60 % of ultimate load at ambient conditions.

small due to the small dimensions of the specimens and the analysis showed that practically no redistribution of stress takes place in these cases, not even for the case with maximum rate of heating. The calculated total strains were also found to be virtually independent of the rate of heating when plotted against the characteristic temperature, and, accordingly, the use of a characteristic temperature in the previous discussion must be regarded as sufficiently accurate.

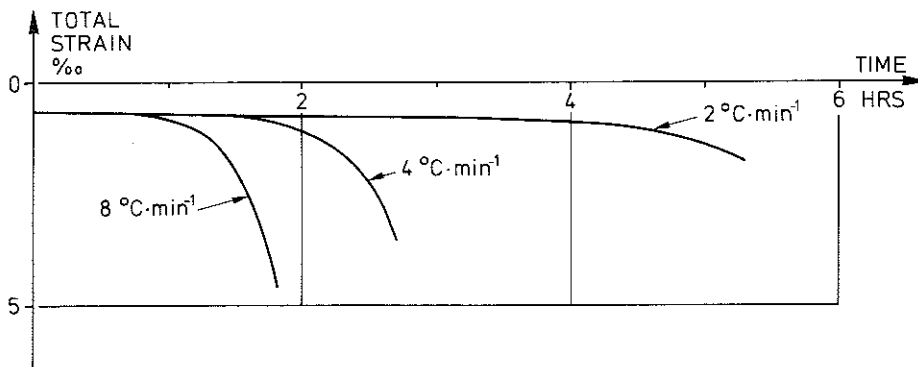


Fig 49 Calculated total strains for the cylindrical columns referred to in fig 46, as a function of time.

6

CONCLUSIONS

The mechanical behaviour of loaded concrete under transient high-temperature conditions is considerably different from that observed under steady-state temperature conditions. The compressive strains induced by compressive stresses are much greater during heating than at constant temperature. This is valid for the first heating - for subsequent cycles the behaviour is different.

A constitutive law valid at transient conditions can be formulated in terms of four strain components, thermal strain, instantaneous stress-related strain, creep (as measured at constant temperature and constant stress) and transient strain. The transient strain is an important component in the model, accounting for the deformations occurring under stress upon a temperature rise. This component accounts for the difference in behaviour between transient and steady-state temperature conditions and is normally considerably greater than both the stress-related strain and the creep strain components.

The constitutive model developed in this paper reflects the actual behaviour in a very appropriate way and can easily be applied in a computer analysis of thermally exposed concrete structures. Quantitatively, the model is developed for a specified concrete mixture, with quartzite aggregate. But it is reasonable to assume that it is qualitatively valid for a wide range of concretes if the variation in temperature of the thermal expansion, the strength and the ultimate strain can be estimated. A more appropriate modelling for a particular concrete is obtained if the transient strain component can be estimated from tests where specimens are heated to failure under sustained load. Accordingly, further experimental investigations of concrete at high temperatures should in the first place involve this type of test.

The general implication of the model is that the stresses created in concrete upon first heating due to differential or restrained thermal expansion are very insignificant or even nonexistent. Such stresses can not themselves contribute to compression failure. It is furthermore obvious that an elastic stress distribution bears little resemb-

lance to reality and is virtually meaningless even as a rough qualitative estimate.

The suggested model is especially important for problems like statically indeterminate concrete structures and slender columns under thermal exposure, where an accurate estimate of the deformations is necessary.

REFERENCES

- /1/ Magnusson, S.E., Pettersson, O., Thor, J., "Fire Engineering Design of Steel Structures (Brandteknisk dimensionering av stålkonstruktioner)", Manual, issued by the Swedish Institute of Steel Construction, Stockholm, 1974 - English edition, Lund and Stockholm, 1976.
- /2/ Anderberg, Y., Pettersson, O., Thelandersson, S., Wickström, U., "A Differentiated Design of Fire Exposed Concrete Structures", presented at FIP VII Congress, New York, 1974.
- /3/ Anderberg, Y.- Thelandersson, S., Stress and Deformation Characteristics of Concrete at High Temperatures 1. General Discussion and Critical Review of Literature. Div. of Structural Mechanics and Concrete Construction, Lund Institute of Technology, Bulletin No. 34, Lund, Sweden, 1973.
- /4/ Thelandersson, S., Mechanical Behaviour of Concrete under Torsional Loading at Transient, High-Temperature Conditions. Div. of Structural Mechanics and Concrete Construction, Lund Institute of Technology, Bulletin No. 46, Lund, Sweden 1974.
- /5/ Illston, J.M., Sanders, P.D. , The Effect of Temperature Change Upon the Creep of Mortar Under Torsional Loading. Mag. of Concrete Research, Vol. 25, No. 84, Sept 1973.
- /6/ Nishizawa, N., Okamura, H., Strength and Inelastic Properties of Concrete at Elevated Temperature. Concrete for Nuclear Reactors, ACI SP - 34, Detroit 1972.
- /7/ Skinner, D.H., Measurement of High Temperature. Properties of Steel, BHP Melbourne Research Laboratories, May 1972.
- /8/ Ödeen, K., Nordström, Å., Termiska egenskaper hos betong vid höga temperaturer (Thermal Properties of Concrete at High Temperatures). Cement och Betong 1972:1, Stockholm.

- /9/ Weigler, H., Fischer, R., Beton bei Temperaturen von 100° C bis 750° C. Beton, 2, Februari 1968.
- /10/ Schneider, U., Zur Kinetik Festigkeitsmindernder Reaktionen in Normalbetonen bei hohen Temperaturen. Dissertation, Technische Universität, Braunschweig, Dec. 1973.
- /11/ Schneider, U., Kordina, K., Über das Verhalten von Normalbeton unter stationären und instationären Temperaturbeanspruchung. 3rd International Conference on Structural Mechanics in Reactor Technology, Vol. 3, Part H, H:116, London 1975.
- /12/ Cruz, C.R. Elastic Properties of Concrete at High Temperatures. Journal of the PCA Res. and Dev. Lab, Jan 1966.
- /13/ Furamura, F. The Stress-strain Curve of Concrete at High Temperature. Tokyo Institute of Technology, Report of Meeting at Architectural Institute of Japan, 1966.
- /14/ Anderberg, Y., Fire-exposed Hyperstatic Concrete Structures - An Experimental and Theoretical Study. Division of Structural Mechanics and Concrete Construction, Lund Institute of Technology, Bulletin 55, Lund 1976.
- /15/ Becker, J., Bresler, B., Fires - R.C.A Computer Program for the Fire Response of Structures - Reinforced Concrete Frames. University of California, Berkeley, Fire Research Group 74-3, July 1974.
- /16/ Sargin, M., Handa, V. K., A General Formulation for the Stress-strain Properties of Concrete. Solid Mechanics Division, University of Waterloo, Waterloo, Ontario, Canada, Report No.3, May 1969.
- /17/ Thelandersson, S., Effect of High Temperatures on Tensile Strength of Concrete. Nordisk Betong No. 2, 1972.